The Pennsylvania State University
APPLIED RESEARCH LABORATORY
P.O. Box 30
State College, PA 16804

ANGLE SAMPLE VARIANCE OF AZIMUTHALLY SPREAD SCATTERING PROCESSES, USING A TWO-ELEMENT ARRAY

by

J. R. Johnescu
D. W. Ricker

Technical Report No. TR 90-009
July 1990

Supported by:
Space and Naval Warfare Systems Command

L.R. Hettche, Director
Applied Research Laboratory

Approved for public release; distribution unlimited

REPORT DOCUMENTATION PAGE

Form Approved
OMB No. 0704-0188

1. AGENCY USE ONLY (Leave blank)	2. REPORT DATE	3. REPORT TYPE AND DATES COVERED
	July 1990	

4. TITLE AND SUBTITLE

Angle Sample Variance of Azimuthally Spread Scattering Processes, Using a Two-Element Array

5. FUNDING NUMBERS

6. AUTHOR(S)

J. R. Johnescu, D. W. Ricker

7. PERFORMING ORGANIZATION NAME(S) AND ADDRESS(ES)

Applied Research Laboratory
The Pennsylvania State University
P. O. Box 30
State College, PA 16804

8. PERFORMING ORGANIZATION REPORT NUMBER

TR 90-009

9. SPONSORING / MONITORING AGENCY NAME(S) AND ADDRESS(ES)

Space and Naval Warfare Systems Command
Department of the Navy
Washington, DC 20363-5100

10. SPONSORING / MONITORING AGENCY REPORT NUMBER

N-00039-88-C-0051

11. SUPPLEMENTARY NOTES

12a. DISTRIBUTION / AVAILABILITY STATEMENT

Unlimited

12b. DISTRIBUTION CODE

13. ABSTRACT *(Maximum 200 words)*

Active echo energy received by a two-element array may be comprised of both spatially coherent and spatially spread scattering processes (such as clutter or reverberation) and isotropic noise. Such inputs may be filtered by a correlation receiver from which range, Doppler and angle estimates can be made. In many cases, these estimates display azimuthal support, such that angle estimates of spatially spread scattering processes are stochastically distributed across the array beamwidth, whereas angle estimates of spatially coherent scattering processes tend to be azimuthally compact.

A scattering function model is used to relate the geometry and scattering distributions to the angle estimation problem when a two-element array is used as the receiver. The angle estimate statistics are described by probability density functions which depend upon array geometry, scattering distribution, scattering strength and ambient noise. At low levels of interference, spatially coherent scattering processes display low angle variance. Consequently, realizations of measured angle from spatially compact processes tend to

14. SUBJECT TERMS

array, scattering function model, receiver, acoustics, Monte Carol, probability density function

15. NUMBER OF PAGES

78

16. PRICE CODE

17. SECURITY CLASSIFICATION OF REPORT	18. SECURITY CLASSIFICATION OF THIS PAGE	19. SECURITY CLASSIFICATION OF ABSTRACT	20. LIMITATION OF ABSTRACT
UNCLASSIFIED	UNCLASSIFIED	UNCLASSIFIED	SAR

13. Abstract (continued)

be consistent while those from spread scatters tend to be distributed across the receive beam support. When multiple measurements of angle are available, the sample variance can be useful as a means to characterize the underlying scattering distribution.

Probability density function sof angle sample variance as a function of coherent scattered energy, diffuse scattered energy and ambient noise are developed through a multistep statistical transformation and verified with Monte Carlo estimations. Errors intorudced by assumptions regarding correlation between angle measurement realizations are discussed and examples are provided.

ABSTRACT

Active echo energy received by a two-element array may be comprised of both spatially coherent and spatially spread scattering processes (such as clutter or reverberation) and isotropic noise. Such inputs may be filtered by a correlation receiver from which range, Doppler and angle estimates can be made. In many cases, these estimates display azimuthal support, such that angle estimates of spatially spread scattering processes are stochastically distributed across the array beamwidth, whereas angle estimates of spatially coherent scattering processes tend to be azimuthally compact.

A scattering function model is used to relate the geometry and scattering distributions to the angle estimation problem when a two-element array is used as the receiver. The angle estimate statistics are described by probability density functions which depend upon array geometry, scattering distribution, scattering strength and ambient noise. At low levels of interference, spatially coherent scattering processes display low angle variance. Consequently, realizations of measured angle from spatially compact processes tend to be consistent while those from spread scatterers tend to be distributed across the receive beam support. When multiple measurements of angle are available, the sample variance can be useful as a means to characterize the underlying scattering distribution.

Probability density functions of angle sample variance as a function of coherent scattered energy, diffuse scattered energy and ambient noise are developed through a multistep statistical transformation and verified with Monte Carlo estimations. Errors introduced by assumptions regarding correlation between angle measurement realizations are discussed and examples are provided.

TABLE OF CONTENTS

TABLE OF CONTENTS (CONTINUED)

LIST OF FIGURES

LIST OF FIGURES (CONTINUED)

LIST OF SYMBOLS

c speed of sound in medium

CIR acronym for Coherent-to-Incoherent Component Ratio

d distance between array elements

DTFT acronym for Discrete Time Fourier Transform

E_I received incoherent process energy

E_S received coherent process energy

E_0 transmitted process energy

edf acronym for empirical distribution function

epd acronym for Electrical Phase Difference

$E\{\phi\}$ mean of single realization of ϕ

FFT acronym for Fast Fourier Transform

f_C received coherent process

f_{C1} received coherent process at first element of two-element array

f_{C2} received coherent process at second element of two-element array

f_I received incoherent process

f_{I1} received incoherent process at first element of two-element array

f_{I2} received incoherent process at second element of two-element array

f_R received process

$f_{S^2_\phi}(S^2_\phi)$ density function for the third convolution of section 3.2.1.7 (subtraction), i.e. angle sample variance

$\overline{f_{S^2_\phi}(S^2_\phi)}$ angle sample variance density function mean

f_t transmitted process

$f_u(u)$ density function for the first transformation of section 3.2.1.1 (division)

LIST OF SYMBOLS (continued)

$f_v(v)$ density function for the second convolution of section 3.2.1.3 (subtraction)

$f_w(w)$ density function for the second transformation of section 3.2.1.4 (subtraction)

$f_y(y)$ density function for the third transformation of section 3.2.1.5 (subtraction)

$f_z(z)$ density function for the third convolution of section 3.2.1.6 (subtraction)

$f_\phi(\phi)$ density function for the electrical phase difference

$f_{\bar{\phi}}(\bar{\phi})$ density function for the first convolution of section 3.2.1.2 (summation), i.e. sample angle mean

h impulse response filter

i sample number

I_1 real component of complex process L_1

I_2 imaginary component of complex process L_1

I_3 real component of complex process L_2

I_4 imaginary component of complex process L_2

k_0 variable proportional to the CIR

L filter output

L_{I1} incoherent process component of filter output for first element of two-element array

L_{I2} incoherent process component of filter output for second element of two-element array

L_{s1} coherent process component of filter output for first element of two-element array

L_{s2} coherent process component of filter output for second element of two-element array

L_1 filter output of first element of two-element array

LIST OF SYMBOLS (continued)

L_2 filter output of second element of two-element array

N number of samples

n noise process (complex white Gaussian)

NBCW acronym for Narrowband Continuous Wave

$N_{a,b}$ vectors

N_0 energy contained in noise process

$N_{1,3}$ real components of vectors $N_{a,b}$

$N_{2,4}$ imaginary components of vectors $N_{a,b}$

n_1 noise component of first element of two-element array

n_2 noise component of second element of two-element array

pdf acronym for Probability Density Function

R scattering process range support

$\vec{r}_C$ three-dimensional position vector of a spatially coherent scattering process f_C

R_{I0} incoherent process scattering strength per unit delay and angle

$\vec{r}_I$ three-dimensional position vector of a spatially scattering process f_I

$\vec{r}_R$ three-dimensional position vector of a receive aperture

R_S scattering function

R_{SI} incoherent process scattering function

R_{SC} coherent process scattering function

R_{C0} coherent process scattering strength

$\vec{r}_s$ three-dimensional position vector of any scattering process

$\vec{r}_t$ three-dimensional position vector of the transmit aperture

LIST OF SYMBOLS (continued)

S spreading function

S_C zero Doppler coherent process spreading function

S_S zero Doppler spreading function

S_I zero Doppler incoherent process spreading function

S_ϕ^2 random variable for fourth transformation of section 3.2.1.7 (division), i.e. angle sample variance

t time

T filter pulse duration interval

T_s scattering strength of coherent and incoherent processes

u random variable for first transformation of section 3.2.1.1 (division)

u_r unit vector in direction of receiver

u_s unit vector in direction of scattering process

u_t unit vector in direction of transmitter

v random variable for second convolution of section 3.2.1.3 (subtraction)

W transmit channel bandwidth

w random variable for second transformation of section 3.2.1.4 (scaling)

w_r receive array weighting

w_t transmit array weighting

x variable

y random variable for third transformation of section 3.2.1.5 (squaring)

z random variable for third convolution of section 3.2.1.6 (summation)

β mathematical variable relating k_0, electrical phase difference and most probable electrical phase difference

LIST OF SYMBOLS (continued)

Δt FFT/IFFT sampling interval

θ angle of a scattering process

$\hat{\theta}$ hypothesized angle

θ_b receive beamwidth

θ_s azimuthal support of a scattering process

θ_0 point scatterer angle

λ_0 wavelength of scattering process return

$\mu_{i,j}$ row i, column j component of covariance matrix

π mathematical constant *pi* ≈ 3.14159265

σ_ϕ^2 variance of a single realization of ϕ

τ round trip delay

$\hat{\tau}$ hypothesized delay

τ_0 point scatterer round trip delay

ϕ electrical phase difference

$\overline{\phi}$ random variable for first convolution of section 3.2.1.2 (summation), i.e. sample angle mean

ϕ_i i^{th} sample of electrical phase difference

ϕ_0 most probable electrical phase difference

ϕ_1 electrical phase of first element in two-element array

ϕ_2 electrical phase of second element in two-element array

ψ_b arithmetic variable which relates point scatterer angle and wavelength

ψ_0 arithmetic variable which relates receive beamwidth and wavelength

Ω_r receive aperture

LIST OF SYMBOLS (continued)

Ω_s scattering region

Ω_t transmit aperture

Ω_{SI} spatially spread scattering region

Ω_{SS} spatially coherent scattering region

Ω_u scattering region in direction u_s

ω_d angular Doppler shift

ω_0 angular frequency of scattering process return

Chapter 1

INTRODUCTION

1.1 Background

Active echo energy received by a two-element array may be comprised of both spatially coherent, and spatially spread scattering processes (such as clutter or reverberation) and isotropic noise. Such inputs may be filtered by a correlation receiver from which range, Doppler and angle estimates can be made. In many cases, these estimates display azimuthal support, such that angle estimates of spatially spread scattering processes are stochastically distributed across the array beamwidth, whereas, angle estimates of spatially coherent scattering processes tend to be azimuthally compact. Signals can be designed to meet specific requirements in relation to scattering process characteristics, geometry, medium conditions and desired ambiguity resolution.[7] Early accomplishments in this area were made by Rihaczek,[20] VanTrees[23] and Woodward,[25] and significant on-going work is being carried out by Altes and Titlebaum,[1] Costas,[5] Golomb and Taylor,[8] Green[9] and Titlebaum.[21]

Spatial support is defined as the range (delay) and azimuthal (angle) distributions of a scattering process. Spatial support can either be coherent (compact), wherein a scattering process occupies a small region in range and azimuth, or diffuse, wherein the scattering process is spread in range and across the receiver beamwidth. Estimates of range and angle from scattering processes exhibit random variations dependent upon the amount of spatial support of the scattering processes and the coherent-to-incoherent component ratio (CIR). These variations

may be described by probability density functions.[10] It should be recognized that many other factors contribute to the specific form of such density functions, such as[3,26]

1. transmitted frequency,
2. physics of scattering process,
3. medium temperature, pressure and flow,
4. number of transmitter/scatterer/receiver paths,
5. noise, and
6. density of spatially spread scattering processes.

Both spatially coherent processes, and spatially incoherent processes possess average energy levels and thus a CIR, which may be defined as the ratio of the energy received from the spatially coherent scattering process to the total received incoherent energy level.[26]

1.2 Variance Estimation

The azimuthal spread of a scattering process can be described in terms of an angle pdf, from which the variance may be used as an indicator of azimuthal scattering support. Specifically, spatially coherent scattering processes tend to exhibit low angle variance, whereas spatially spread scattering processes tend to exhibit high angle variance.[10,19]

The goal of this thesis is to provide a means of describing spatial coherence by developing angle sample variance probability density functions which are para-

metrically related to scattering process strength and distribution, noise, number of realizations, and electrical phase difference between receivers of a two-element array.

1.3 Assumptions and Limitations

In deriving the angle sample variance pdf, the following assumptions (including rationale) were made:

1. received processes are composed of narrow-band continuous wave (NBCW) Gaussian processes embedded in noise, which allows for use of the electrical phase difference (angle) pdf developed by Middleton[13] and Rainal,[17]

2. uncorrelated scattering conditions in the medium, which provides uncorrelated returns in range and azimuth, and consequently allows the use of a scattering function model,[19,27]

3. scattering aperture in far field, which allows the received processes to be considered as plane waves,[27]

4. N degrees of freedom (statistically independent angle estimates) for angle sample variance calculation, where N is the number of measurements, which allows the use of convolutions in finding joint statistics,[16]

5. two-element array with finite beamwidth,[17,19]

1.4 Organization

In chapter 2, a scattering function model will be introduced which relates the transmitted and received processes in terms of the temporal and spatial vari-

ations of the medium.[27] The angle pdf, developed by Middleton[13] and Rainal,[17] will be discussed and shown to be dependent upon the spatially coherent scattering strength and angle, the spatially spread scattering strength and distribution, and the noise level.[10]

The angle pdf is used in chapter 3 to derive the angle sample variance pdf, which is developed theoretically with a multistep transformation model and verified with Monte Carlo estimates. The angle sample variance density function will be shown to exhibit a low mean value when dominated by a spatially coherent process embedded in low-level spread scattering and noise.

In chapter 4 the Monte Carlo method is further utilized to demonstrate effects of correlation between the angle sample mean and angle sample variance, i.e. when there are $N-1$ degrees of freedom for the angle sample variance calculation. The results will illustrate the effects of assumption (4) in section 1.3.

Chapter 5 contains conclusions and recommendations for further work.

Chapter 2

ANGLE ESTIMATION OF SCATTERING PROCESSES

2.1 Introduction

In this chapter, the theoretical basis for the relationship of angle variance to azimuthal coherence will be presented. This is achieved by using a linear scattering model to relate the phase across a two-element array to the azimuthal distribution of scattered energy described by a scattering function. It will be shown that phase variance is proportional to the angular spread of the scattered energy and inversely proportional to the CIR, and generally, a relatively small value of phase variance may be taken as an indicator of backscatter which is dominated by a spatially coherent (small angular spread) scattering process.

2.2 Background

Prior to investigating specific relations of azimuthal variance, background information will be presented. In section 2.2.1, the echolocation relations of Middleton[13] and the spreading function fundamentals of Laval[10] and Ziomek[26,27] provide the bases for a linear model of scattering processes. These relations are extended in section 2.2.2 to include scattering process geometry and correlation between the transmitted process, and the received coherent and incoherent processes. The phase difference between array elements is related to the electrical phase difference (epd) probability density function (pdf) of Middleton[13] and Rainal,[17] in section 2.2.3. Based upon these fundamentals, the magnitude of the azimuthal (angle) variations can be related to the electrical phase difference pdf, as per Ricker,[19] in section 2.3.

2.2.1 Linear Backscatter Model

In this section, the scattering process components will be introduced. It will be shown that a scattering process can be represented by a linear filter described in terms of time and position, which in turn can be represented by a spreading function. The spreading function is used to represent a scattering process as a filter response in terms of time delay and Doppler. A general expression will be developed which expresses the received process in terms of the transmitted process strength, spreading function and backscatter geometry.

The backscatter process under consideration will be assumed to be composed of a spatially coherent (angularly compact) scattering process, a spatially spread scattering process and random uncorrelated noise, in the far field of the source. In modelling the time and position relations of these three mechanisms, the received input can be written as

$$f_r(t,\vec{r}_r) = f_C(t,\vec{r}_C) + f_I(t,\vec{r}_I) + n, \tag{2.1}$$

where

f_r - the received process,

f_C - the spatially coherent scattering process (small angular support),

f_I - the spatially spread scattering process (clutter or reverberation),

n - complex narrowband isotropic uncorrelated white Gaussian noise (WGN), and

$\vec{r}_{r,C,I}$ - three-dimensional position vector of each of these processes.

In an echolocation sense, reflections from scattering processes (spatially coherent or diffuse) can be envisioned pictorially, for a bistatic receiver, as demonstrated in figure 2.1.[14] The symbols $\vec{u}_r$, $\vec{u}_s$ and $\vec{u}_t$ designate unit vectors in the direction of the receiver, the scattering process and transmitter, respectively. The signal path from a scattering process is the collection of ray paths originated from the transmitter which first reflect from the scattering region and then are incident upon the receiver. The term "ray paths" is used to denote that signal paths may experience refraction and several reflections, but are nonetheless the process reflected from a scattering process. The scattering processes can either be spatially coherent (compact) or spatially spread. The noise n will be assumed to be a complex narrowband white Gaussian noise process with spectral density N_0.[3,22]

Assuming a linear transmission medium, the scattering process can be viewed as a time-variant, space-variant impulse response filter.[19] The function $h(\tau, t, \vec{u}_s)$ is the response of the filter at time t to a unit impulse applied τ seconds ago at the origin and reflected from a scattering site Ω_S with direction $\vec{u}_s$, and range $|\vec{r}_s|$. The filter response will be assumed to be uncorrelated in delay τ and direction $\vec{u}_s$, and to be wide sense stationary in time. If the process transmitted from the origin at time $t - \tau$ is $f_t(t - \tau)$ and the process received at the origin at time t is $f_r(t)$, then the incremental filter response can be written as

$$f_r(t, \vec{u}_s, \tau) = f_t(t - \tau) h(\tau, t, \vec{u}_s) d\tau d\Omega_u \tag{2.2}$$

where Ω_u is an incremental area representing the support of the direction vector $\vec{u}_s$. Using a trajectory diagram,[18,21] to account for delays caused by the transmitter

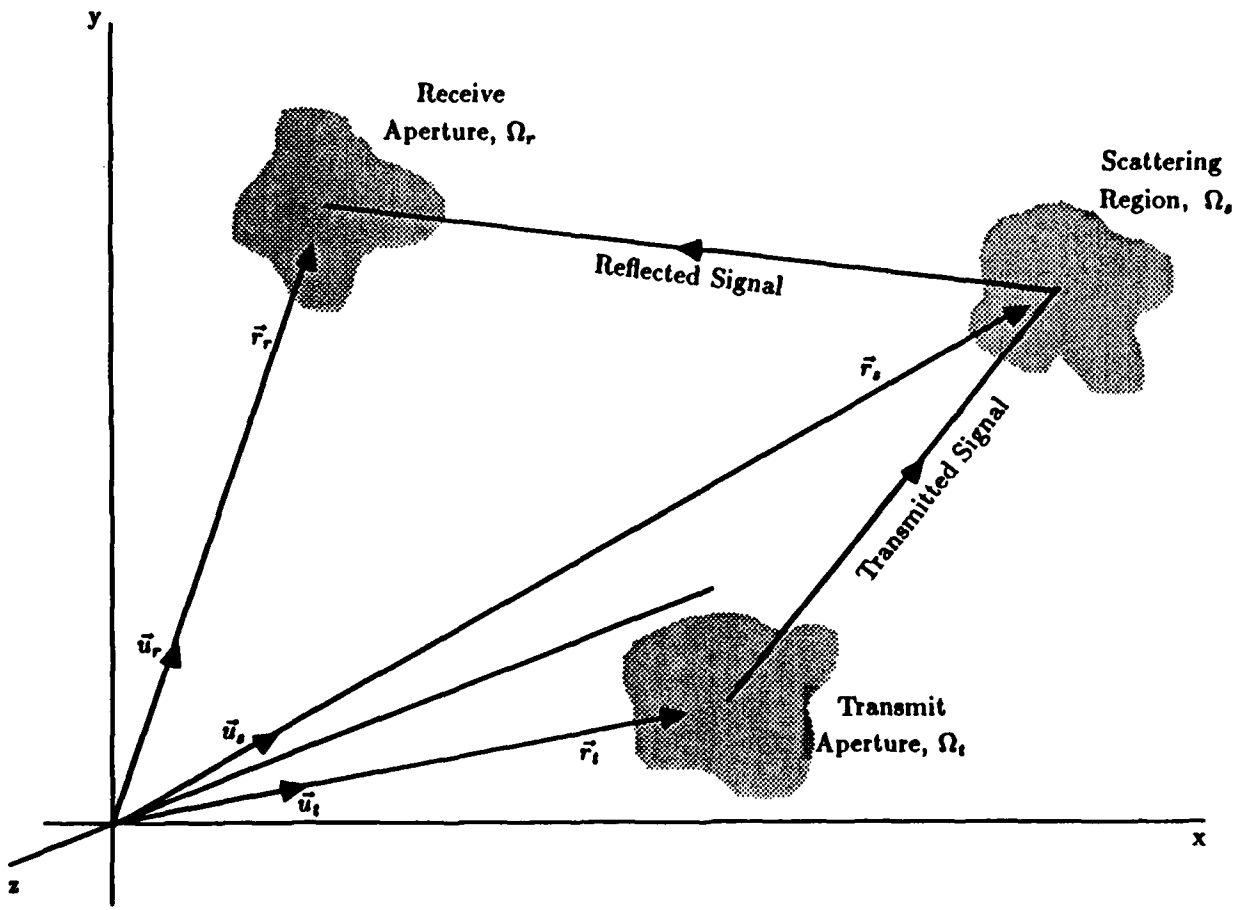

Figure 2.1

Echolocation of a Scattering Process[14]

and receiver locations with respect to the scattering process direction, results in

$$f_r(t,\vec{u}_s,\tau) = f_t\Big(t + \frac{\vec{u}_s}{c}\cdot(\vec{r}_r+\vec{r}_t) - \tau\Big)h\Big(\tau, t + \frac{\vec{r}_r\cdot\vec{u}_s}{c}, \vec{u}_s\Big)\,d\tau d\Omega_u. \tag{2.3}$$

Including transmit beam steering (where u_0 denotes the transmit energy direction), the transmitted energy E_0, transmit/receive array weighting ($w_t(\vec{r}_t)$ and $w_r(\vec{r}_r)$ respectively), and integrating over the transmit aperture and scattering support, results in

$$f_r(t,\vec{r}_r) = \sqrt{E_0}w_r(\vec{r}_r)\int_{\Omega_t}\int_{\Omega_u}\int_{\tau} f_t\Big(t + \frac{\vec{r}_r\cdot\vec{u}_s}{c} - \frac{\vec{r}_t\cdot(\vec{u}_0-\vec{u}_s)}{c} - \tau\Big)\,w_t(\vec{r}_t)$$
$$h\Big(\tau, t + \frac{\vec{r}_r\cdot\vec{u}_s}{c}, \vec{u}_s\Big)\,d\tau\,d\Omega_u\,d\Omega_t. \tag{2.4}$$

Equation 2.4 represents stochastic realizations at a point receiver located at $\vec{r}_r$, resulting from a linear space-time stochastic operation in the direction $\vec{u}_s$, upon the transmitted waveform $f_t(t)$ which originated at the location $\vec{r}_t$.[19] The symbol Ω_t designates the support of the transmit aperture.

Given an impulse response in time and position, it is useful to describe the amount of spreading of a scattering process in terms of Doppler, time and position. One such representation is the spreading function which will in this case be defined as the Fourier transform of the impulse response with respect to time only, i.e.[26]

$$h(\tau,t,\vec{u}_s) = F_t^{-1}\Big\{S(\tau,\omega_d,\vec{u}_s)\Big\}. \tag{2.5}$$

Consequently, equation 2.4 can be expressed in terms of the spreading function as

$$f_r(t,\vec{r}_r) = \sqrt{E_0} w_r(\vec{r}_r) \int_{\Omega_t} \int_{\Omega_u} \int_{\tau} \int_{\omega_d} f_t\Big(t + \frac{\vec{r}_r \cdot \vec{u}_s}{c} - \frac{\vec{r}_t \cdot (\vec{u}_0 - \vec{u}_s)}{c} - \tau\Big) w_t(\vec{r}_t)$$
$$S(\tau, \omega_d, \vec{u}_s) exp\Big\{ j\omega_d \Big(t + \frac{\vec{r}_r \cdot \vec{u}_s}{c}\Big)\Big\}\, d\omega_d\, d\tau\, d\Omega_u\, d\Omega_t. \tag{2.6}$$

The following assumptions will be made with regards to the angle statistics of spatially discrete versus spread scattering,

1. uncorrelated scattering in $\tau, \vec{u}_s$,
2. transmission beamwidth is greater than the scattering support in angle,
3. no Doppler spreading, such that the spreading function can be expressed as $S_S(\tau, \omega_d, \vec{u}_s) = S(\tau, \vec{u}_s)\delta(\omega_d - \omega_0)$, where ω_0 is the transmit angular frequency,
4. unity transmit/receive weighting, and
5. monostatic transmitter/receiver at origin.

At the expense of additional complexity, these assumptions can be removed. Given these assumptions, equation 2.6 can be expressed in terms of the spreading function as

$$f_r(t,\vec{r}_r) = \sqrt{E_0} \int_{\Omega_S} \int f_t\Big(t + \frac{\vec{u}_s \cdot \vec{r}_r}{c} - \tau\Big) S_S(\tau, \vec{u}_s) d\tau d\Omega_u, \tag{2.7}$$

which represents an echo return observed at time t and position $\vec{r}_r$ in terms of the transmitted process and energy spreading in the medium. Using this expression, the processes received from spatially coherent and spread scatterers can be

modelled separately as

$$f_C(t,\vec{r}_r) = \sqrt{E_0}\int_{\Omega_{SS}}\int f_t\Big(t+\frac{\vec{u}_s\cdot\vec{r}_r}{c}-\tau\Big)S_C(\tau,\vec{u}_s)d\tau d\Omega_u \qquad (2.8)$$

$$f_I(t,\vec{r}_r) = \sqrt{E_0}\int_{\Omega_{SI}}\int f_t\Big(t+\frac{\vec{u}_s\cdot\vec{r}_r}{c}-\tau\Big)S_I(\tau,\vec{u}_s)d\tau d\Omega_u \qquad (2.9)$$

where $S_C(\tau,\vec{u}_s)$ and $S_I(\tau,\vec{u}_s)$ are the zero Doppler spreading functions for the coherent and incoherent processes, respectively, and the integration is over the scattering regions, Ω_{SS} and Ω_{SI} for the spatially coherent and spread scattering processes, respectively.[19]

2.2.2 Correlation Processing with Two-Element Array

It will be assumed that one or more continuous wave processes are transmitted and the resulting backscatter is incident upon a two-element array at the origin as shown in figure 2.2.[19] The scattering region is confined to finite spatial support Ω_S in azimuth θ_S and range R. The two receiver inputs are filtered, and the phase difference between the channels is measured. This type of receiver is referred to as a phase comparison receiver and is shown in figure 2.3.[17]

Using equations 2.8 and 2.9, and assuming a narrowband continuous wave (NBCW) transmitted process $f_t(t) = exp(j\omega_0 t)$ and array geometry of figure 2.2, the spatially coherent and incoherent processes at each receiver input can be expressed as[19]

$$f_{C1,C2}(t) = \sqrt{E_0}\int_{\Omega_{SS}}\int exp\Big\{j\omega_0\Big(t\pm\frac{d\theta}{2c}-\tau\Big)\Big\}S_C(\tau,\theta)d\tau d\theta \qquad (2.10)$$

$$f_{I1,I2}(t) = \sqrt{E_0}\int_{\Omega_{SI}}\int exp\Big\{j\omega_0\Big(t\pm\frac{d\theta}{2c}-\tau\Big)\Big\}S_I(\tau,\theta)d\tau d\theta, \qquad (2.11)$$

where the small angle approximation is used for $\sin\theta$. The return energy time

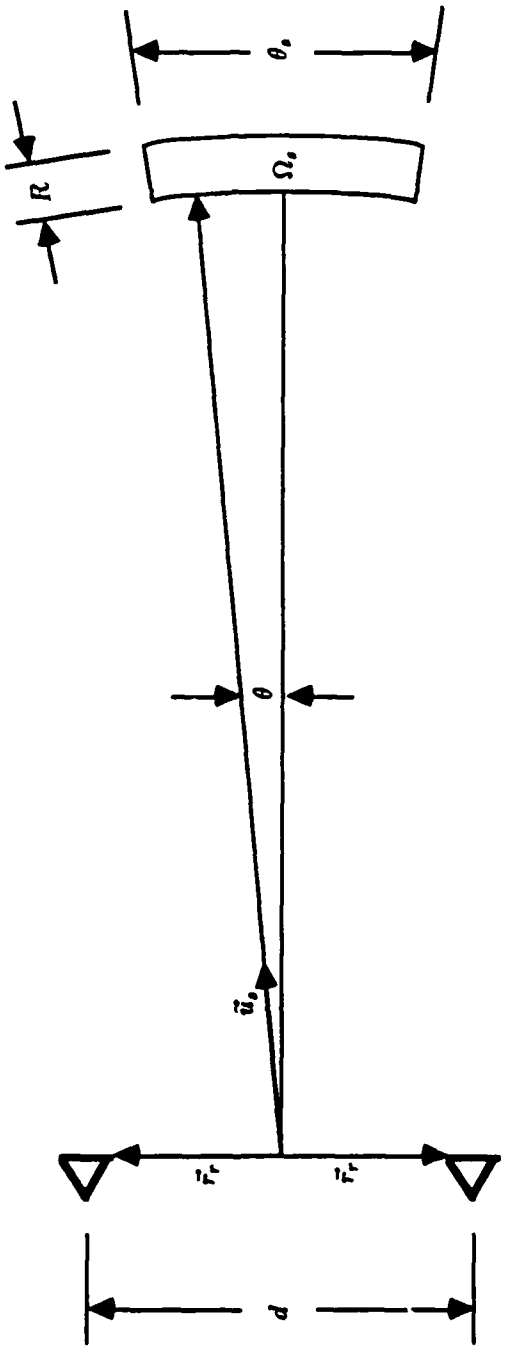

Figure 2.2

Scattering Process/Two-Element Array Geometry[19]

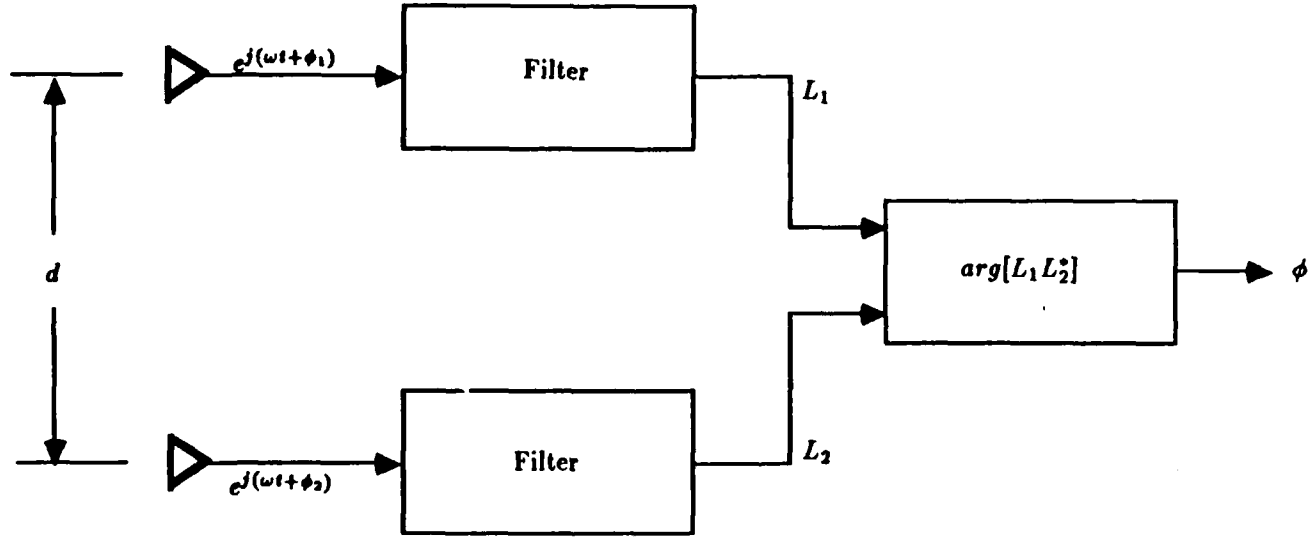

Figure 2.3

Two-Element Array Phase Comparison Receiver[17]

series for each array element is filtered using a replica of the transmitted process which includes a hypothesized delay $\hat{\tau}$ and angle $\hat{\theta}$. The symbol " $\hat{}$ " designates hypothesis. For a narrowband process with pulse duration T, the filter is[6]

$$L = \frac{1}{T}\int_{-\infty}^{+\infty} f(t \pm \frac{d\theta}{2c} - \tau) f^*(t \pm \frac{d\hat{\theta}}{2c} - \hat{\tau}) dt, \tag{2.12}$$

Denoting the filtered coherent and incoherent processes as L_{S1}, L_{S2}, L_{I1} and L_{I2}, the outputs at phase centers 1 and 2 are;[19]

$$L_{S1,S2}(\hat{\theta},\hat{\tau}) = \sqrt{E_0}\int_{\Omega_{SS}}\int exp\ j\Big\{\pm\frac{\pi d(\theta-\hat{\theta})}{\lambda_0} - \omega_0(\Delta\tau)\Big\} S_C(\tau,\theta)\, d\tau\, d\theta, \tag{2.13}$$

$$L_{I1,I2}(\hat{\theta},\hat{\tau}) = \sqrt{E_0}\int_{\Omega_{SI}}\int exp\ j\Big\{\pm\frac{\pi d(\theta-\hat{\theta})}{\lambda_0} - \omega_0(\Delta\tau)\Big\} S_I(\tau,\theta)\, d\tau\, d\theta, \tag{2.14}$$

where

$$\Delta\tau = \tau - \hat{\tau}, \tag{2.15}$$

$$\lambda_0 = \frac{2\pi c}{\omega_0}. \tag{2.16}$$

2.2.3 Electrical Phase Difference pdf

Using equation 2.1, the net complex filter output of the two elements are[18]

$$L_1 = L_{S1} + L_{I1} + n_1, \tag{2.17}$$

$$L_2 = L_{S2} + L_{I2} + n_2. \tag{2.18}$$

The functions L_1 and L_2 are complex Gaussian random variables, from which the electrical phase difference may be computed as

$$\phi = arg[L_1 L_2^*]. \tag{2.19}$$

The probability density function (pdf) for ϕ, i.e. between two complex Gaussian NBCW processes, is given by Middleton[13] and Rainal[17] as

$$f_\phi(\phi) = \frac{1-k_0^2}{2\pi}(1-\beta^2)^{-3/2}\left[\beta \arcsin(\beta) + \frac{\pi\beta}{2} + \sqrt{1-\beta^2}\right], \tag{2.20}$$

where

$$\beta = k_0 cos(\phi - \phi_0), \tag{2.21}$$

$$\phi_0 = tan^{-1}\left[\frac{\mu_{14}}{\mu_{13}}\right], \tag{2.22}$$

$$k_0^2 = \frac{\mu_{13}^2 + \mu_{14}^2}{\mu_{11}\mu_{44}}. \tag{2.23}$$

The term $\mu_{i,j}$ is computed from a 4 X 4 covariance matrix,[17] wherein

$$\mu_{i,j} = E\{I_i, I_j\}, \tag{2.24}$$

where[19]

$$I_1 = Re[L_1], \tag{2.25}$$

$$I_2 = Im[L_1], \tag{2.26}$$

$$I_3 = Re[L_2], \tag{2.27}$$

$$I_4 = Im[L_2]. \tag{2.28}$$

The most probable electrical phase difference between the two inputs is denoted as ϕ_0, where $-\pi \leq \phi_0 \leq +\pi$, and the symbol k_0 is proportional to the relative strength of the coherent component, where $0 \leq k_0 < 1$. It is assumed that the transducers are ideally phase matched such that ϕ represents the actual electrical phase difference between the two inputs. The epd pdf is shown in figure 2.4 for values of k_0 from 0.0 (uniform scattering) to 0.9 (dominant azimuthally coherent

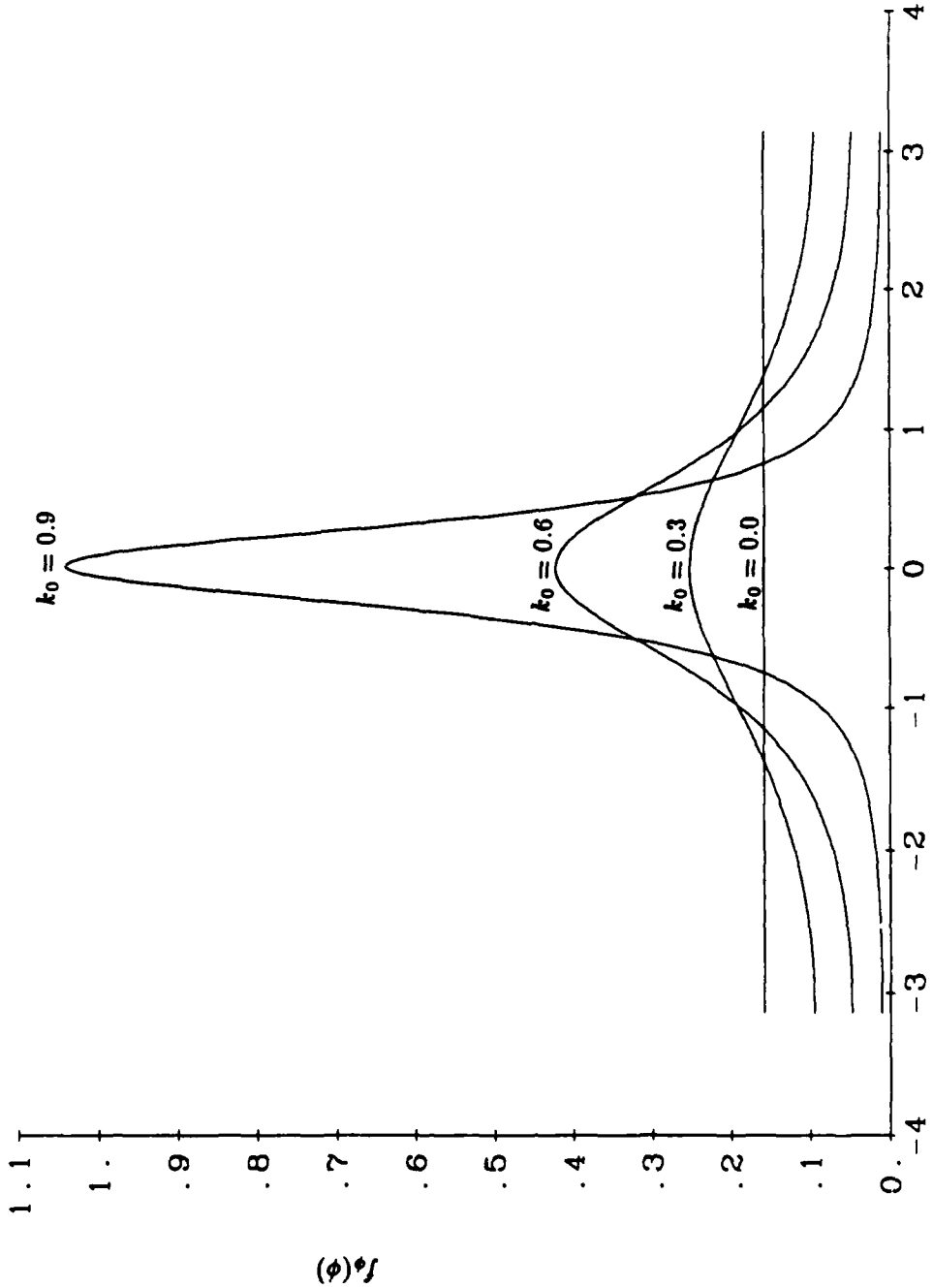

Figure 2.4

$f_\phi(\phi)$, Electrical Phase Difference pdf between correlated narrowband Gaussian processes for $\phi_0 = 0.0$ and $k_0 = 0.0$ through 0.9 in 0.3 increments

scattering). The scattering process angle can be computed from the electrical phase difference by the relation[17]

$$\theta = \sin^{-1}\left(\frac{c\phi}{w_0 d}\right). \tag{2.29}$$

Based upon equation 2.29, the terms electrical phase difference and angle will be used interchangeably.

The electrical phase difference mean and variance are given by Merchant[12] as

$$E\{\phi\} = \frac{\arccos(k_0 \cos\phi_0)}{\sqrt{1 - k_0^2 \cos^2\phi_0}} k_0 \sin\phi_0, \tag{2.30}$$

$$\sigma_\phi^2 = \frac{\pi^2}{12} - \frac{k_0^2}{2} + \arccos(k_0 \cos\phi_0)^2 \frac{(1 - k_0^2)}{(1 - k_0^2 \cos^2\phi_0)}. \tag{2.31}$$

Plots of the epd mean and variance as a function of k_0 and ϕ_0 are given in figures 2.5 and 2.6, respectively.

Without loss of generality, this thesis will be concerned solely with the sample variance when $\phi_0 = 0$. When the azimuthally coherent scattering process is not at $\phi = 0$, the epd pdf is altered such that ϕ_0 and k_0 in equations 2.22 and 2.23, respectively, take on different values dependent upon the correlation between receivers. Correlation effects upon ϕ_0 and k_0 are discussed by Merchant, p. 29.[12] Since (1) the epd pdf is symmetric about ϕ_0 and (2) only the variance about ϕ_0 is to be considered, ϕ_0 shall be fixed at 0 and only the parameter k_0 shall be considered.

2.3 Relation of Angle Spread to Azimuthal Scattering Coherency

In section 2.2.3 (figure 2.4), it was shown that k_0, which is proportional to CIR, plays a dominant role in defining the epd pdf. In this section, k_0 will

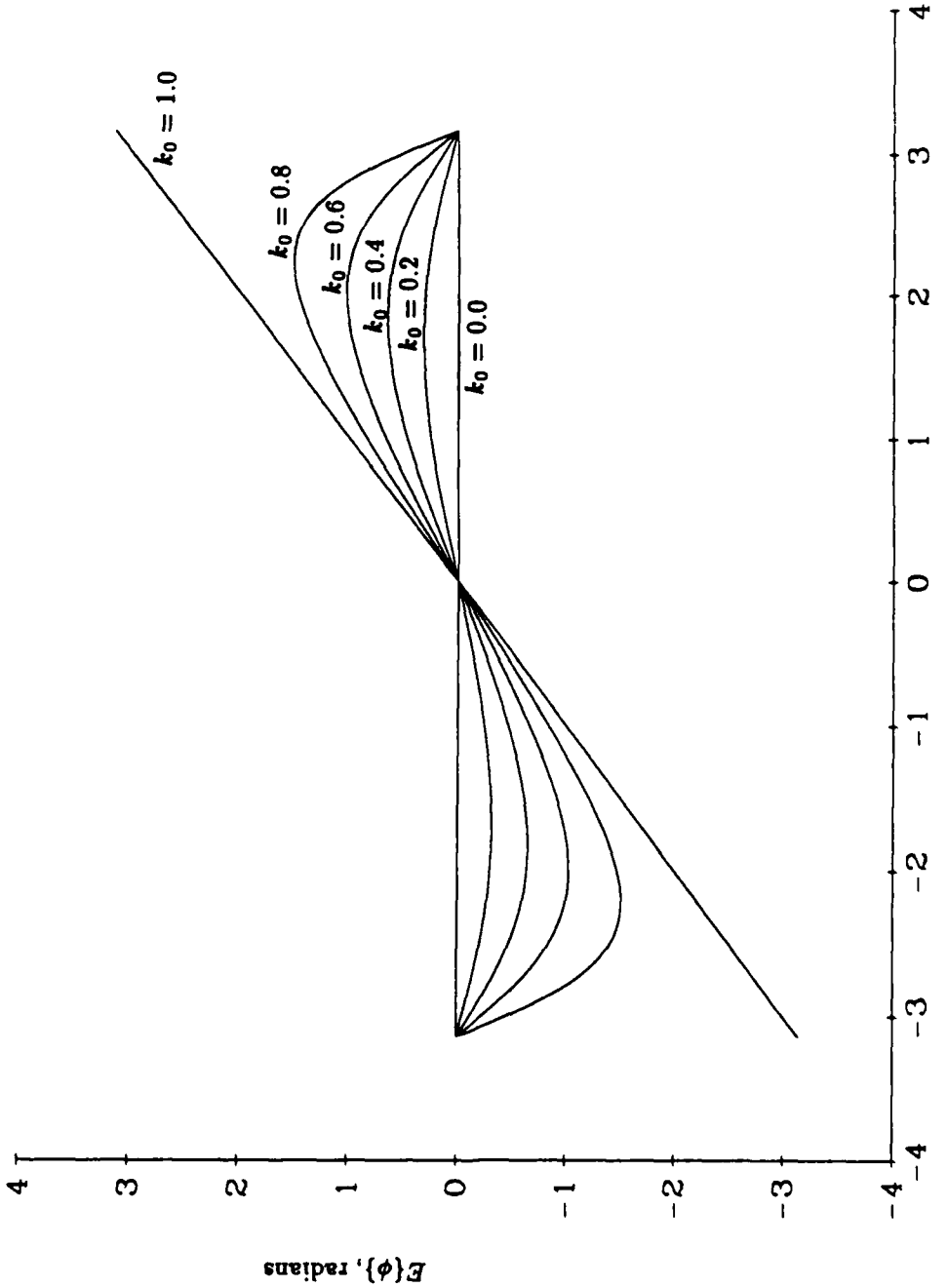

Figure 2.5

Mean of ϕ for a Single Electrical Phase Difference Estimate for $k_0 = 0.0$ through 1.0 [12]

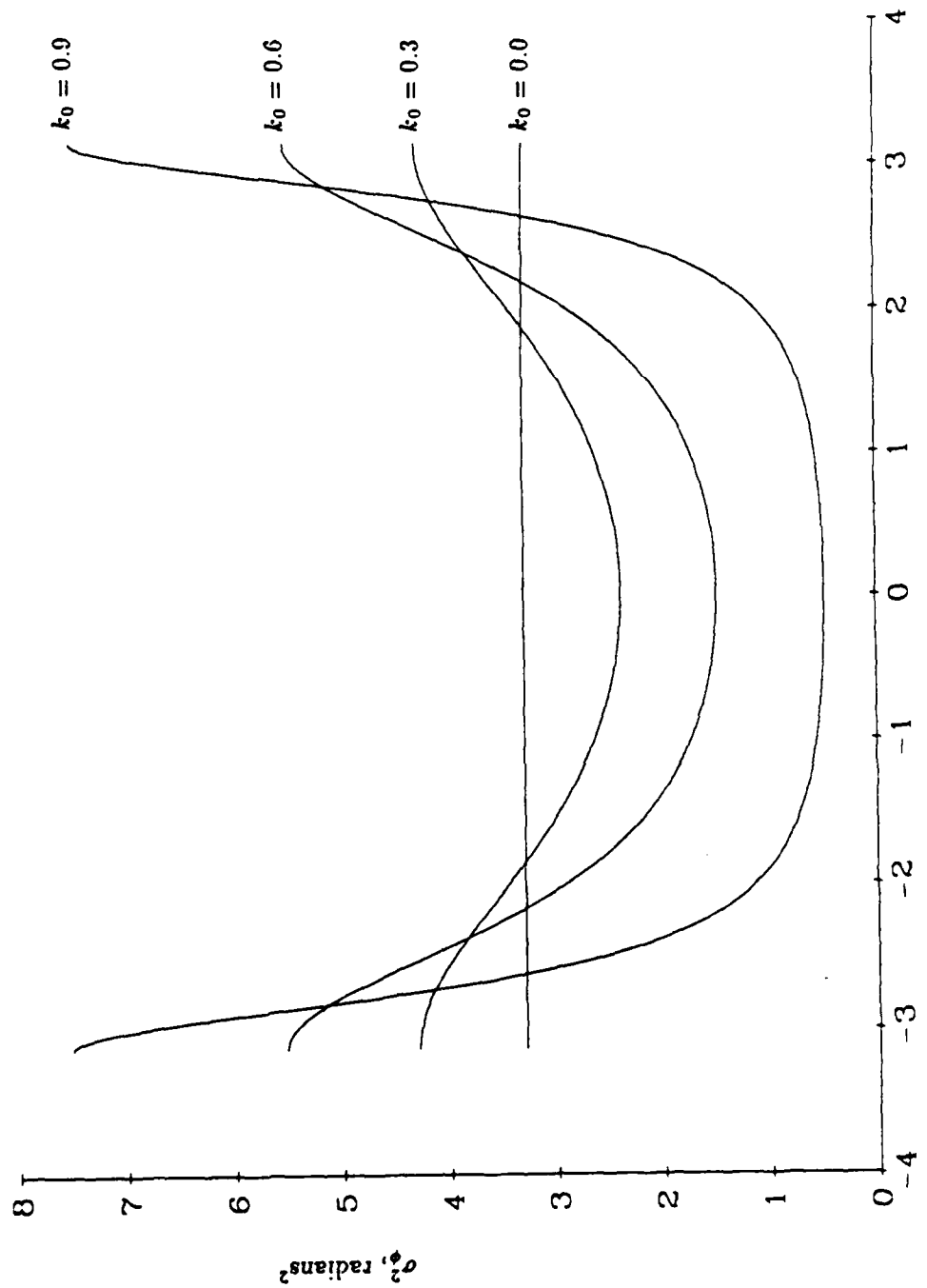

Figure 2.6

Variance of ϕ for a Single Electrical Phase Difference Estimate for $k_0 = 0.0$ through 0.9 [12]

be related to the coherent and incoherent process scattering functions to illustrate the variance of angle estimates from a two-element array when a spatially coherent scattering process is embedded in spatially diffuse backscatter. It will be shown that under low noise, a spatially coherent scattering process exhibits low epd variance.

Assuming uncorrelated scattering, the scattering function $R_S(\tau, \omega_d, \vec{u}_s)$ is the mean-square value of the spreading function, i.e.[26]

$$R_S(\tau, \omega_d, \vec{u}_s) = E\Big\{|S(\tau, \omega_d, \vec{u}_s)|^2\Big\}, \tag{2.32}$$

which in effect is the average amount of spread that the scattered energy will undergo as a function of time delay τ, frequency ω_d, and direction $\vec{u}_s$.[15] Assuming zero Doppler spread, the component scattering functions can be expressed as[27]

$$R_{SC}(\tau, \theta) = E\Big\{|S_C(\tau, \theta)|^2\Big\}, \tag{2.33}$$

$$R_{SI}(\tau, \theta) = E\Big\{|S_I(\tau, \theta)|^2\Big\}. \tag{2.34}$$

Equations 2.22 and 2.23 can be expressed in terms of the scattering function as[19]

$$\phi_0 = tan^{-1}\Big(\frac{Q_s}{Q_c}\Big), \tag{2.35}$$

$$k_0^2 = \frac{S_0^2(Q_c^2 + Q_s^2)}{(1 + S_0 T_s)^2}, \tag{2.36}$$

where

$$Q_s = \int_\Omega \int \Big\{(R_{SC}(\tau, \theta) + R_{SI}(\tau, \theta)\Big\} sin\Big[(\frac{2\pi d}{\lambda_0})(\theta - \hat{\theta})\Big] d\tau d\theta, \tag{2.37}$$

$$Q_c = \int_\Omega \int \Big\{(R_{SC}(\tau, \theta) + R_{SI}(\tau, \theta)\Big\} cos\Big[(\frac{2\pi d}{\lambda_0})(\theta - \hat{\theta})\Big] d\tau d\theta. \tag{2.38}$$

The symbol S_0 is the transmit signal-to-noise ratio (SNR = $\frac{E_0}{N_0}$), and the symbol T_s represents the total combined scattering strengths of the coherent and incoherent processes and is given by

$$T_s = \int_\Omega \int [R_{SC}(\tau,\theta) + R_{SI}(\tau,\theta)] d\tau \, d\theta, \tag{2.39}$$

where the regions of integration are confined by the pulse duration T utilized in filtering the data for τ and the small angle approximation of equations 2.10 and 2.11 for θ. It should be recognized that equations 2.35 and 2.36 are the fundamental relations between the scattering processes and the epd pdf.

2.3.1 Example

For the purpose of illustration, the following example may be used to highlight the effects of CIR and scattering spread upon the epd pdf, and specifically, the epd variance. Assuming uncorrelated scattering, a simple model of the coherent and incoherent process scattering functions may be constructed. Given a point scattering process with constant delay τ_0 and angle θ_0, the coherent process scattering function can be expressed as[19]

$$R_{SC}(\tau,\theta) = R_{C0}\delta(\tau - \tau_0)\delta(\theta - \theta_0), \tag{2.40}$$

where R_{C0} is the coherent process scattering strength. A simple model for the incoherent process scattering function, results from the following assumptions,[17]

1. uniform scattering over the integration time T and

2. uniform angle spread over the receive beamwidth θ_b,

and can be written as[19]

$$R_{SI}(\tau,\theta) = R_{I0}, \text{where } \begin{cases} \tau \in \left[\tau_0 \pm \frac{T}{2}\right] \\ \theta \in \left[\theta_0 \pm \frac{\theta_b}{2}\right] \end{cases}, \tag{2.41}$$

where R_{I0} is the incoherent process scattering strength per unit delay and angle. The incoherent process is assumed to be uniformly distributed within this region. Using E_0 as the transmitted process energy, the received coherent and incoherent process energies realized at the output of the filter are[19]

$$E_S = E_0 R_{C0}, \tag{2.42}$$

$$E_I = E_0 R_{I0} T \theta_b, \tag{2.43}$$

and the noise energy realized at the filter output is N_0. Using the equations 2.37 through 2.39 with $\hat{\theta} = 0$ and the scattering functions defined in equations 2.40 and 2.41, and assuming a rectangular beam pattern, the most probable epd can be shown to be[19]

$$\phi_0 = tan^{-1}\left[\frac{E_S sin(\psi_0)}{E_S cos(\psi_0) + E_I sinc(\psi_b)}\right], \tag{2.44}$$

where

$$\psi_0 = \frac{2\pi\theta_0 d}{\lambda_0}, \tag{2.45}$$

$$\psi_b = \frac{\pi\theta_b d}{\lambda_0}, \tag{2.46}$$

with d as the two-element array width and λ_0 as the wave length. The CIR parameter squared k_0^2 is given by[19]

$$k_0^2 = \frac{E_S^2 + 2E_S E_I \cos(\psi_0) sinc(\psi_b) + E_I^2 sinc^2(\psi_b)}{(N_0 + E_S + E_I)^2}. \tag{2.47}$$

The *sinc* functions in equations 2.44 and 2.47 come about because of the idealized rectangular beam pattern.

From the expression 2.44, it can be seen that the most probable electrical phase is biased by the incoherent process but not the uncorrelated noise. At high CIR, ϕ_0 approaches the phase difference consistent with the point scatterer angle. At low CIR, the bias depends upon the spatial spread of the incoherent process, being small for $\theta_b \geq \frac{\lambda_0}{d}$.[19]

The effect of an increase in noise N_0 or spread scattering support θ_b is to increase the variance of the phase by reducing k_0^2 as can be seen in equation 2.47 and figure 2.3.

Using the model for azimuthally coherent scattering embedded in a diffuse scattering process, the sample variance can be computed from realizations having a pdf given by equation 2.20.

Chapter 3

ANGLE SAMPLE VARIANCE DENSITY FUNCTION

3.1 Introduction

In chapter 2, the electrical phase difference (epd) pdf[13,17] of a two-element array (section 2.2.3), and the inverse relation between epd variance and k_0^2 (section 2.3),[10,19] were illustrated. Angle compactness can now be shown to be measurable by developing the pdf of the angle sample variance. Given the angle sample mean of N samples $\overline{\phi}$, and N statistically independent angle samples ϕ_i, the following relation was used to find the angle sample variance[15]

$$S_\phi^2 = \frac{1}{N-1}\sum_{i=1}^{N}(\phi_i - \overline{\phi})^2. \tag{3.1}$$

Simulation results (figure 3.14) indicate that this estimator is not biased.[4]

The theoretical angle sample variance pdf's will be derived through the use of statistical convolutions and transformations (section 3.2) and verified with Monte Carlo techniques (section 3.3). As discussed in section 2.2.3, only the case of $\phi_0 = 0$ with various values of k_0 will be considered. Effects of statistical correlation between the sample mean and variance will be shown in chapter 4.

3.2 Theoretical Development of Sample Variance

Through convolutions and transformations, a theoretical representation of the angle sample variance pdf, $f_{S_\phi^2}(S_\phi^2)$, can be formed.

3.2.1 Methodology

The angle (epd) sample variance is obtained in seven steps for N samples ($N \geq 2$) by using the continuous pdf of ϕ ($-\pi \leq \phi \leq \pi$). These steps will be shown for $k_0 = 0$, $\phi_0 = 0$ and N = 2 through 6. In section 3.2.2, only the angle sample variance will be shown for $k_0 = 0.5$ and 0.9.

1. Transformation - Division[15,24]

$$u = \frac{\phi}{N}, \text{where } \frac{-\pi}{\mathrm{N}} \leq \mathrm{u} \leq \frac{\pi}{\mathrm{N}} \tag{3.2}$$

2. Convolution - Summation[16]

$$\begin{aligned} \overline{\phi} &= \frac{1}{N}\sum_{i=1}^{N}\phi_i \\ &= \sum_{i=1}^{N} u, \text{where } -\pi \leq \overline{\phi} \leq \pi \end{aligned} \tag{3.3}$$

3. Convolution - Subtraction,[16] ϕ_i and $\overline{\phi}$ are statistically independent

$$v = \phi_i - \overline{\phi}, \text{where } -2\pi \leq \mathrm{v} \leq 2\pi \tag{3.4}$$

4. Transformation - Scaling

$$w = \begin{cases} 2\pi - v, & \text{if } v < -\pi \\ v, & \text{if } -\pi \leq v \leq \pi, \text{ where } -\pi \leq w \leq \pi \\ -2\pi + v, & \text{if } v > +\pi \end{cases} \tag{3.5}$$

5. Transformation - Squaring[15]

$$\begin{aligned} y &= (\phi_i - \overline{\phi})^2 \\ &= w^2, \text{where } 0 < \mathrm{y} \leq \pi^2 \end{aligned} \tag{3.6}$$

6. Convolution - Summation[16]

$$\begin{aligned} z &= \sum_{i=1}^{N} (\phi_i - \overline{\phi})^2 \\ &= \sum_{i=1}^{N} y, \text{where } 0 < z \leq N\pi^2, \end{aligned} \tag{3.7}$$

7. Transformation - Division[15,24]

$$\begin{aligned} S_\phi^2 &= \frac{1}{N-1} \sum_{i=1}^{N} (\phi_i - \overline{\phi})^2 \\ &= \frac{z}{N-1}, \text{where } 0 < S_\phi^2 \leq \frac{N\pi^2}{N-1}. \end{aligned} \tag{3.8}$$

The variables $u, \overline{\phi}, v, w, y, z$ and S_ϕ^2 indicate each step. Note that steps (2.) and (7.) are the sample mean and sample variance of N statistically independent random variables, respectively, and thus given their traditional symbols $\overline{\phi}$ and S_ϕ^2. Given the angle pdf $f_\phi(\phi)$, the pdf of each variable will be found in turn, i.e. $f_u(u) \rightarrow f_{\overline{\phi}}(\overline{\phi}) \rightarrow f_v(v) \rightarrow f_w(w) \rightarrow f_y(y) \rightarrow f_z(z) \rightarrow f_{S_\phi^2}(S_\phi^2)$. Each of these steps is detailed, respectively, in the following subsections.

3.2.1.1 First Transformation, $f_u(u)$

The transformation indicated by equation 3.2 is the initial step in finding the sample mean pdf $f_{\overline{\phi}}(\overline{\phi})$, where the sample mean is given by equation 3.3. Given the angle pdf $f_\phi(\phi)$, a division transformation is carried out as[15,24]

$$f_u(u) = N f_\phi(N\phi). \tag{3.9}$$

Fundamentally, this relation states that the magnitude of $f_\phi(\phi)$ will be increased N-fold and the width decreased N-fold. The pdf's for the division transformation

of a uniformly distributed statistically independent random variable (angle samples at $k_0 = 0$) are shown in figure 3.1. Effectively, the division by N cancels the multiplication by N, and an area of unity is maintained.

3.2.1.2 First Convolution, $f_{\overline{\phi}}(\overline{\phi})$

In this step we wish to find the pdf of the sample mean. The mean of N statistically independent random variables is given in equation 3.3. Since the pdf of the sum of N statistically independent random variables is the convolution of the individual pdf's,[16] the pdf of the angle sample mean is

$$f_{\overline{\phi}}(\overline{\phi}) = f_{u_1}(u_1) * f_{u_2}(u_2) * f_{u_3}(u_3) * \cdots * f_{u_N}(u_N). \tag{3.10}$$

It is assumed that all N samples obey the same pdf, i.e. $f_{u_i}(u_i) = f_u(u)$, and the sample mean pdf becomes

$$f_{\overline{\phi}}(\overline{\phi}) = f_u(u) * f_u(u) * f_u(u) * \cdots * f_u(u), \tag{3.11}$$

which is the N-fold convolution of identical pdf's. Since convolutions in the time domain equate to multiplications in the frequency domain, i.e.

$$f_{u_1}(u_1) * f_{u_2}(u_2) * \cdots * f_{u_N}(u_N) = F^{-1}\Big\{F_{u_1}(u_1) \cdot F_{u_2}(u_2) \cdot \cdots \cdot F_{u_N}(u_N)\Big\}, \tag{3.12}$$

where

$$F_{u_i}(u_i) \equiv F\Big\{f_{u_i}(u_i)\Big\}, \tag{3.13}$$

the angle sample mean pdf $f_{\overline{\phi}}(\overline{\phi})$ can be expressed as

$$f_{\overline{\phi}}(\overline{\phi}) = F^{-1}\{F_u(u) \cdot F_u(u) \cdot \cdots \cdot F_u(u)\}, \tag{3.14}$$

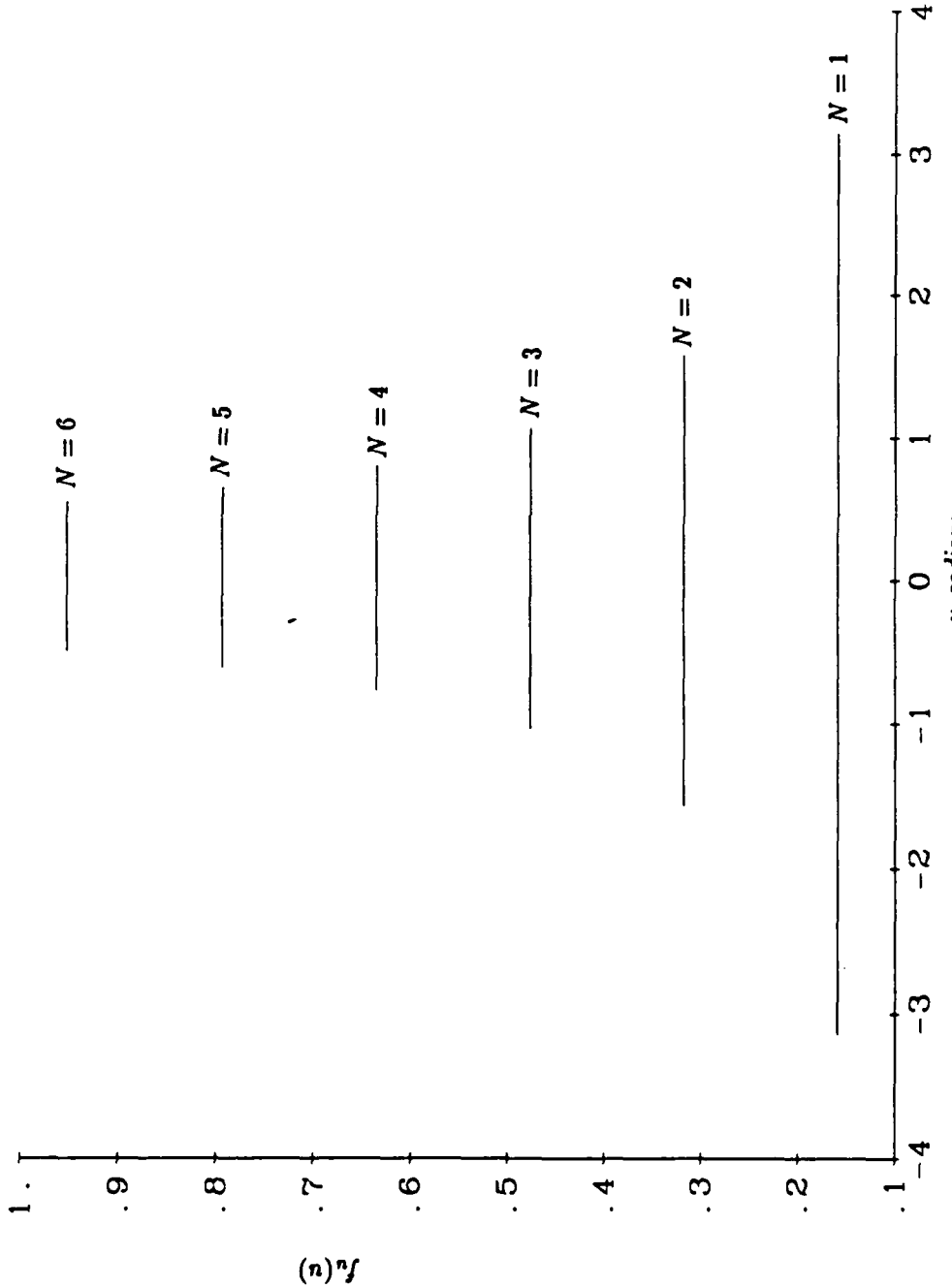

Figure 3.1

$f_u(u)$, Electrical Phase Difference Divided by Number of Samples pdf's for 1 through 6 samples, $k_0 = 0.0$ and $\phi_0 = 0.0$

wherein the number of convolutions is equal to the number of samples.

To preserve the density function area of unity, a discrete-time Fourier transform (DTFT) is utilized, wherein time and frequency samples are normalized by the evenly spaced sampling interval Δt,[6,11] i.e.

$$\Delta t = \frac{t_{max} - t_{min}}{N-1}. \tag{3.15}$$

The DTFT pairs are as follows[11]

$$X(k) = \Delta t \sum_{n=0}^{N-1} x(n) \exp(\frac{-j2\pi kn}{N}), \tag{3.16}$$

$$x(n) = \frac{1}{N\Delta t} \sum_{k=0}^{N-1} X(k) \exp(\frac{j2\pi kn}{N}). \tag{3.17}$$

The sample mean pdf's for 1 through 6 samples are shown in figure 3.2.

3.2.1.3 Second Convolution, $f_v(v)$

Given the mean pdf $f_{\overline{\phi}}(\overline{\phi})$, we can now find the pdf of the difference between a single random sample ϕ_i and the mean of N samples, indicated as v in equation 3.4. The pdf of the difference between two samples is identical to the pdf of the summation of two samples if the samples are statistically independent and their pdf's are symmetric. These are valid assumptions in this case since (1) the epd and epd sample mean pdf's are symmetric about ϕ_0, and (2) the sample mean is assumed statistically independent from the samples about the mean. If

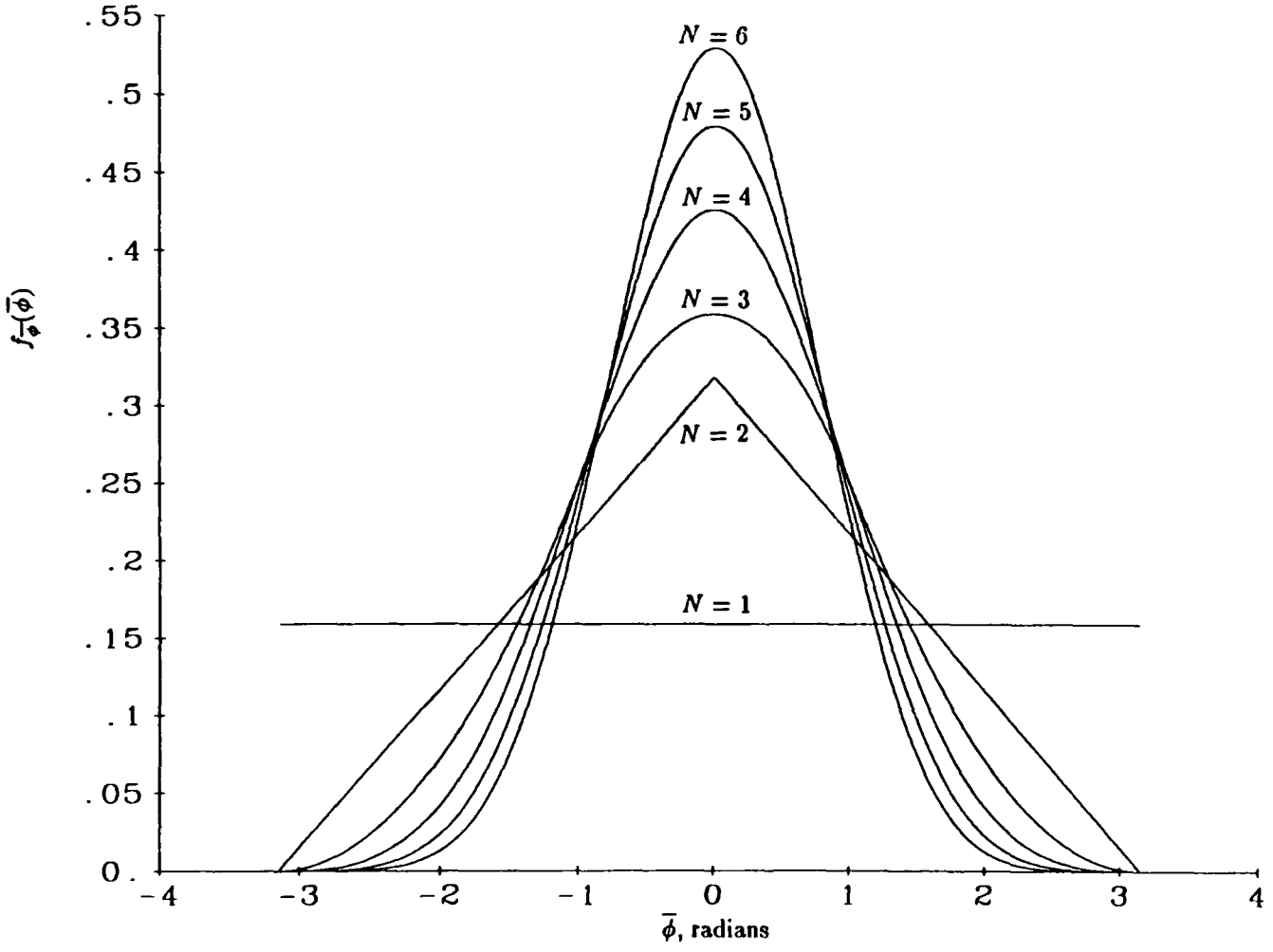

Figure 3.2

$f_{\bar{\phi}}(\bar{\phi})$, Electrical Phase Difference Mean pdf's,
for 1 through 6 samples, $k_0 = 0.0$ and $\phi_0 = 0.0$

$v = \phi + \overline{\phi}$, then the pdf of v can be written as a convolution, i.e.

$$\begin{aligned} f_v(v) &= \int_{-\infty}^{+\infty} f_{\overline{\phi}}(\overline{\phi}) f_\phi(v - \overline{\phi}) d\overline{\phi} \\ &= f_{\overline{\phi}}(\overline{\phi}) * f_\phi(\phi). \end{aligned} \tag{3.18}$$

Deriving a similar expression for $v = \phi - \overline{\phi}$, as per the method shown by Peebles, pp. 102-3,[16] results in

$$f_v(v) = \int_{-\infty}^{+\infty} f_\phi(\phi) f_{\overline{\phi}}(\phi - v) d\phi. \tag{3.19}$$

Since we are only interested in the "difference" between two pdf's, the pdf for $v = \overline{\phi} - \phi$ can be similarly expressed as

$$f_v(v) = \int_{-\infty}^{+\infty} f_{\overline{\phi}}(\overline{\phi}) f_\phi(\overline{\phi} - v) d\overline{\phi}. \tag{3.20}$$

This expression is identical to equation 3.18, except that $f_{\overline{\phi}}(\phi - v)$ is folded about $v = 0$. Thus if $f_{\overline{\phi}}(\overline{\phi}) = f_{\overline{\phi}}(-\overline{\phi})$, i.e. symmetric, equation 3.20 can be expressed as

$$\begin{aligned} f_v(v) &= \int_{-\infty}^{+\infty} f_{\overline{\phi}}(\overline{\phi}) f_\phi(\overline{\phi} - v) d\overline{\phi} \\ &= \int_{-\infty}^{+\infty} f_{\overline{\phi}}(\overline{\phi}) f_\phi(v - \overline{\phi}) d\overline{\phi} \end{aligned}, \tag{3.21}$$

which is identical to equation 3.18, and thus the difference between two symmetric pdf's can be written as a first order convolution, i.e.

$$\begin{aligned} f_v(v) &= f_{\phi - \overline{\phi}}(\phi - \overline{\phi}) \\ &= f_{\overline{\phi}}(\overline{\phi}) * f_\phi(\phi). \end{aligned} \tag{3.22}$$

The resultant pdf's for the example conditions are shown in figure 3.3. Similar to the pdf of the summation of N samples in section 3.2.1.1, the widths of $f_{\overline{\phi}}(\overline{\phi})$

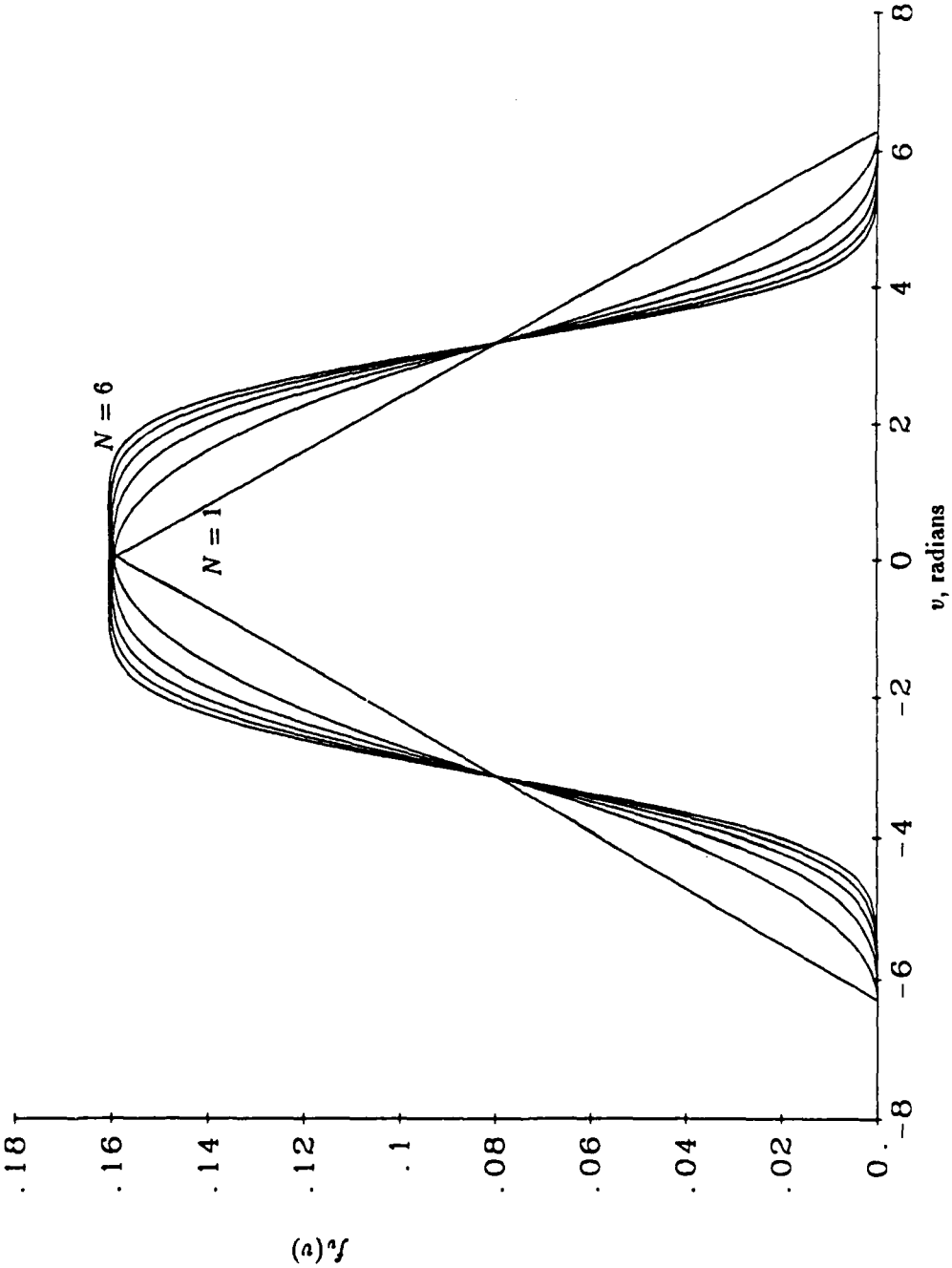

Figure 3.3

$f_v(v)$, Subtraction (Convolution) pdf's,
for 1 through 6 samples, $k_0 = 0.0$ and $\phi_0 = 0.0$

and $f_\phi(\phi)$ are effectively added (doubled) and the mean heights are halved, and thus the area of unity is maintained.

3.2.1.4 Second Transformation, $f_w(w)$

There is one peculiarity for the pdf of the difference between $f_{\overline{\phi}}(\overline{\phi})$ and $f_\phi(\phi)$, which is that we are finding the pdf between two continuous density functions. In other words the pdf's for ϕ_i and $\overline{\phi}$ extend continuously from $-\pi$ to $+\pi$, such that $-\pi = +\pi$. Therefore, a difference about the mean less than $-\pi$ or greater than $+\pi$ must be transformed to the interval $(-\pi, +\pi)$. This can be rephrased as, if $\phi_i - \overline{\phi} < -\pi$, then the result is translated to $(+\pi)$ minus (the amount less than $-\pi$). Similarly, if $\phi_i - \overline{\phi} > +\pi$, then the result is translated to $(-\pi)$ plus (the amount greater than $+\pi$). The transformation is described in *equation* 3.5.

An example is given to highlight this concept. If the mean of N samples is found to be $-\pi$ and an angle sample of $\frac{\pi}{2}$ is taken, then $\phi_i - \overline{\phi} = \frac{\pi}{2} - (-\pi) = +\frac{3\pi}{2}$, which translates to $\frac{-\pi}{2}$. In other words, the difference about the mean is effectively $\frac{-\pi}{2}$ since $+\pi$ and $-\pi$ are the same point of the continuous angle density function.

Such transformations of $f_v(v)$ to $f_w(w)$ for the pdf's of figure 3.3 are shown in figure 3.4. Since the areas less than $-\pi$ and greater than $+\pi$ are added to the existing area between $-\pi$ and $+\pi$, the area of unity is preserved.

Figure 3.4 indicates some amount of error. Since the difference has been found between a uniform distribution and the mean of a continuous uniform distribution, all of the pdf's of figure 3.4 should be uniform. Given a range

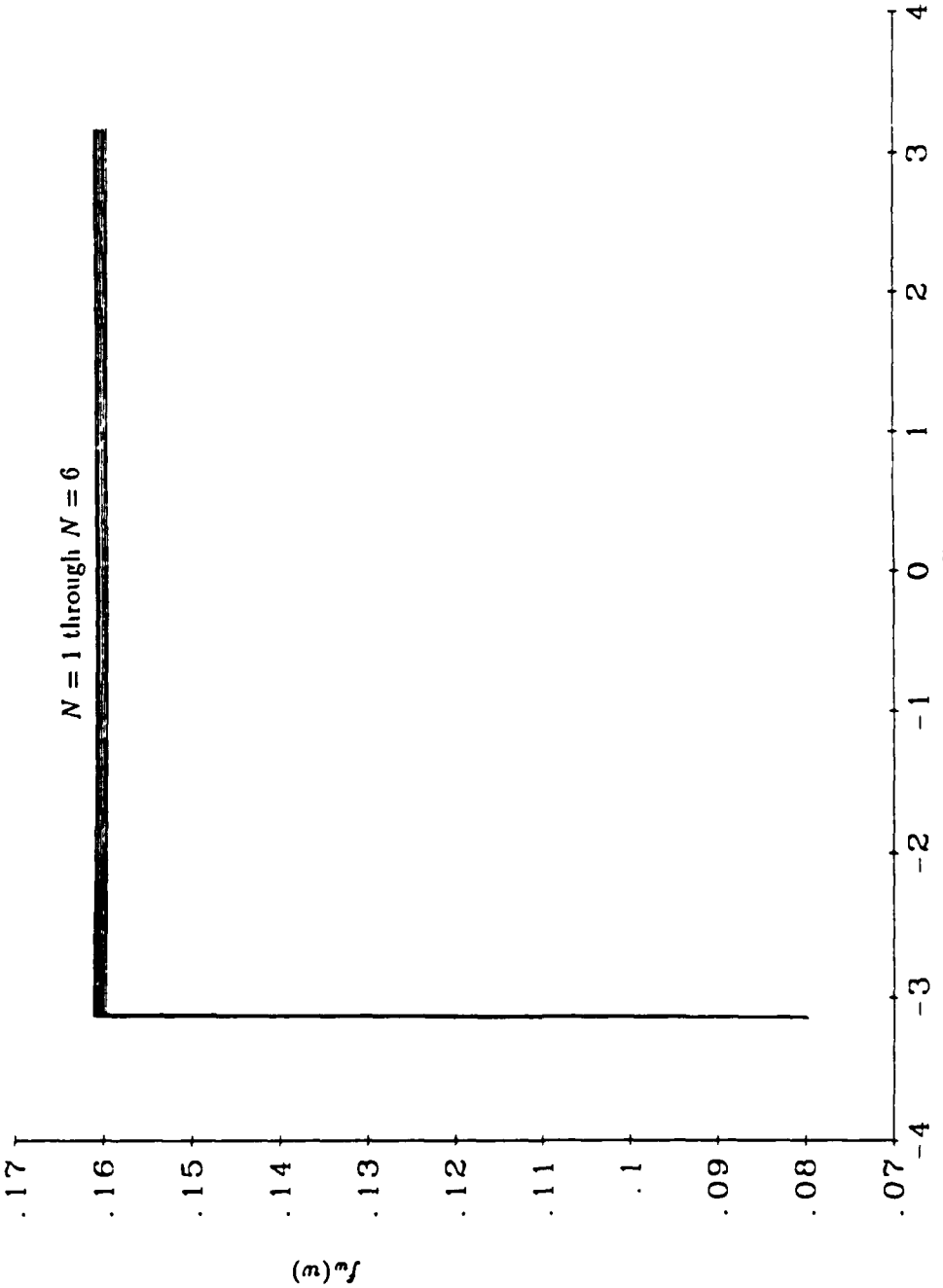

Figure 3.4

$f_w(w)$, Continuity (Transformation) pdf's,
for 1 through 6 samples, $k_0 = 0.0$ and $\phi_0 = 0.0$

from $-\pi$ to $+\pi$, this would indicate a uniform magnitude of $\frac{1}{2\pi} \approx 0.1592$. The curves shown increase in height with each additional sample, ranging in uniform magnitudes from ≈ 0.1598 to 0.1612. These errors are primarily due to FFT degree, DTFT normalization and single precision computations.

The "glitch" appears at $-\pi$ because there was one extra point between -2π and $-\pi$ than between 0 and $+\pi$. This point is disregarded in the next step.

3.2.1.5 Third Transformation. $f_y(y)$

The pdf for the square of the difference about the mean, as per equation 3.6, is a squaring transformation of $f_w(w)$. The squaring transformation is given by[15]

$$f_y(y) = \frac{f_w(-\sqrt{y}) + f_w(+\sqrt{y})}{2\sqrt{y}}. \tag{3.23}$$

If the originating density function is symmetric about the mean, as is the case with $f_w(w)$, i.e. $f_w(-w) = f_w(+w)$, the squaring operation can be rewritten as

$$f_y(y) = \frac{f_w(+\sqrt{y})}{\sqrt{y}}. \tag{3.24}$$

Squaring transformations of $f_w(w)$ of figure 3.4 are shown in figure 3.5. The pdf area of unity is preserved.

3.2.1.5.1 Discretization of $f_w(w)$

Prior to the summation (convolution) of the next section, the samples of $f_y(y)$ must be evenly spaced. In section 3.2.1.2, it was emphasized that before performing a convolution, the time domain samples must be evenly spaced. With

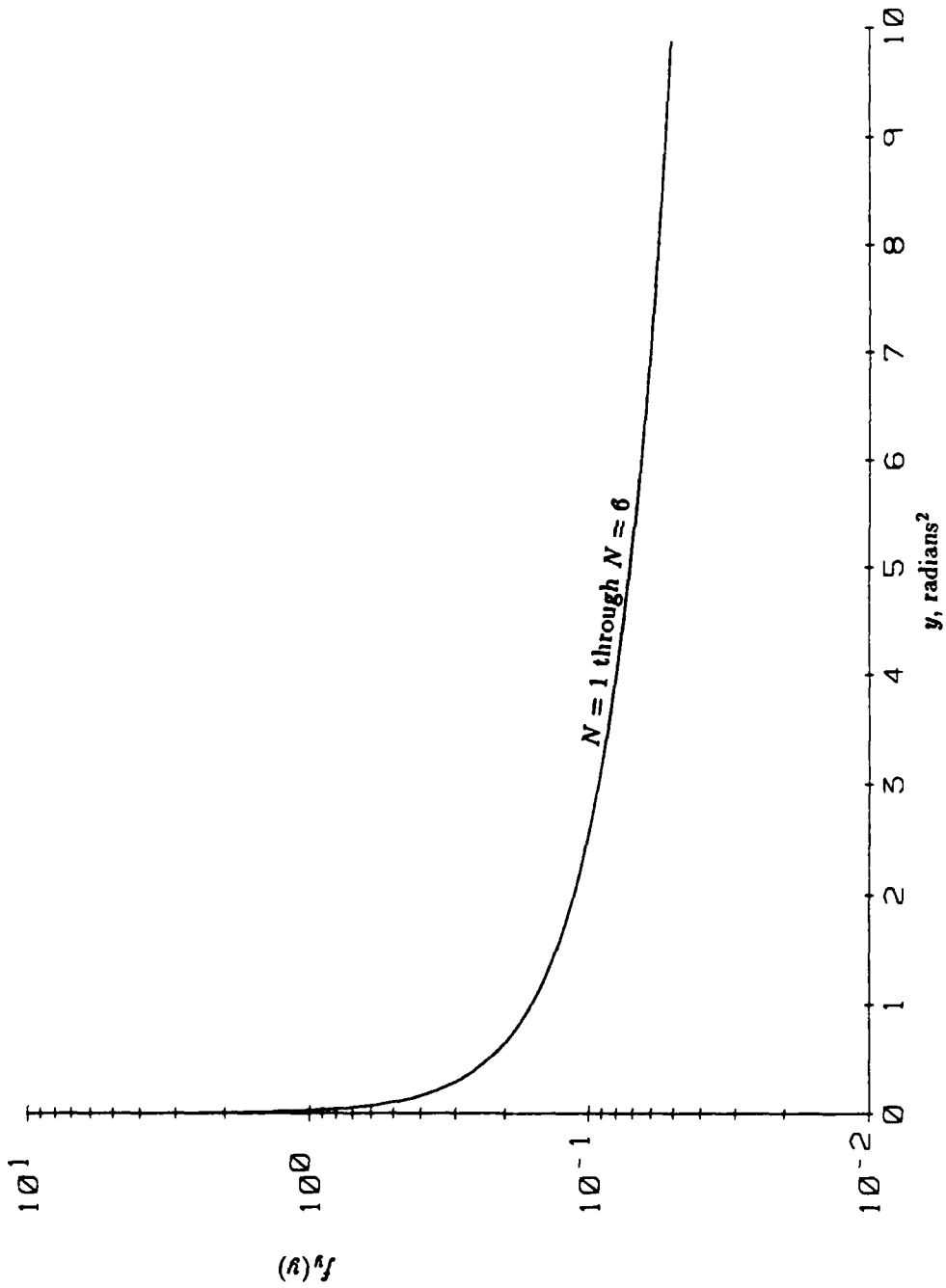

Figure 3.5

$f_y(y)$, Squaring (Transformation) pdf's,
for 1 through 6 samples, $k_0 = 0.0$ and $\phi_0 = 0.0$

the squaring operation of the last section, such even spacing has been lost. Thus, before doing the summation operation in section 3.2.1.6, it is imperative that the squared samples be evenly spaced. This can be effectively done through regression techniques.[2] As shown in figure 3.5 the pdf's of $(\phi_i - \overline{\phi})^2$ exhibit extremely steep slopes close to the ordinate axis, i.e. approach $-\infty$, which is unfavorable to regression techniques and consequently the variance model. This effect becomes more extreme as the k_0 increases. Therefore, in modelling the variance density function, regression was performed upon the step prior to the squaring operation $f_w(w)$, wherein the slopes were not extreme. The discretization operation was carried out as follows:

1. evenly spaced points were found between 0 and π^2 (the limits of y),

2. square roots of these values were taken and assigned as abscissa values of w, and

3. regression was performed prior to the squaring operation to find the corresponding ordinate axis values of each new abscissa value (a third order polynomial with five points per regression packet was found to give the least deviation).[2]

Thus, given evenly spaced abscissa values, convolutions of $f_y(y)$ can be performed.

3.2.1.6 Third Convolution, $f_z(z)$

It was shown in section 3.2.1.2 that the pdf of the sum of N statistically independent samples is equal to the convolution of their individual pdf's.[16] Figure 3.6 illustrates the convolution of N $f_y(y)$'s given by equation 3.24. The erratic curves around an ordinate axis magnitude of 10^{-6} exhibit the error caused by

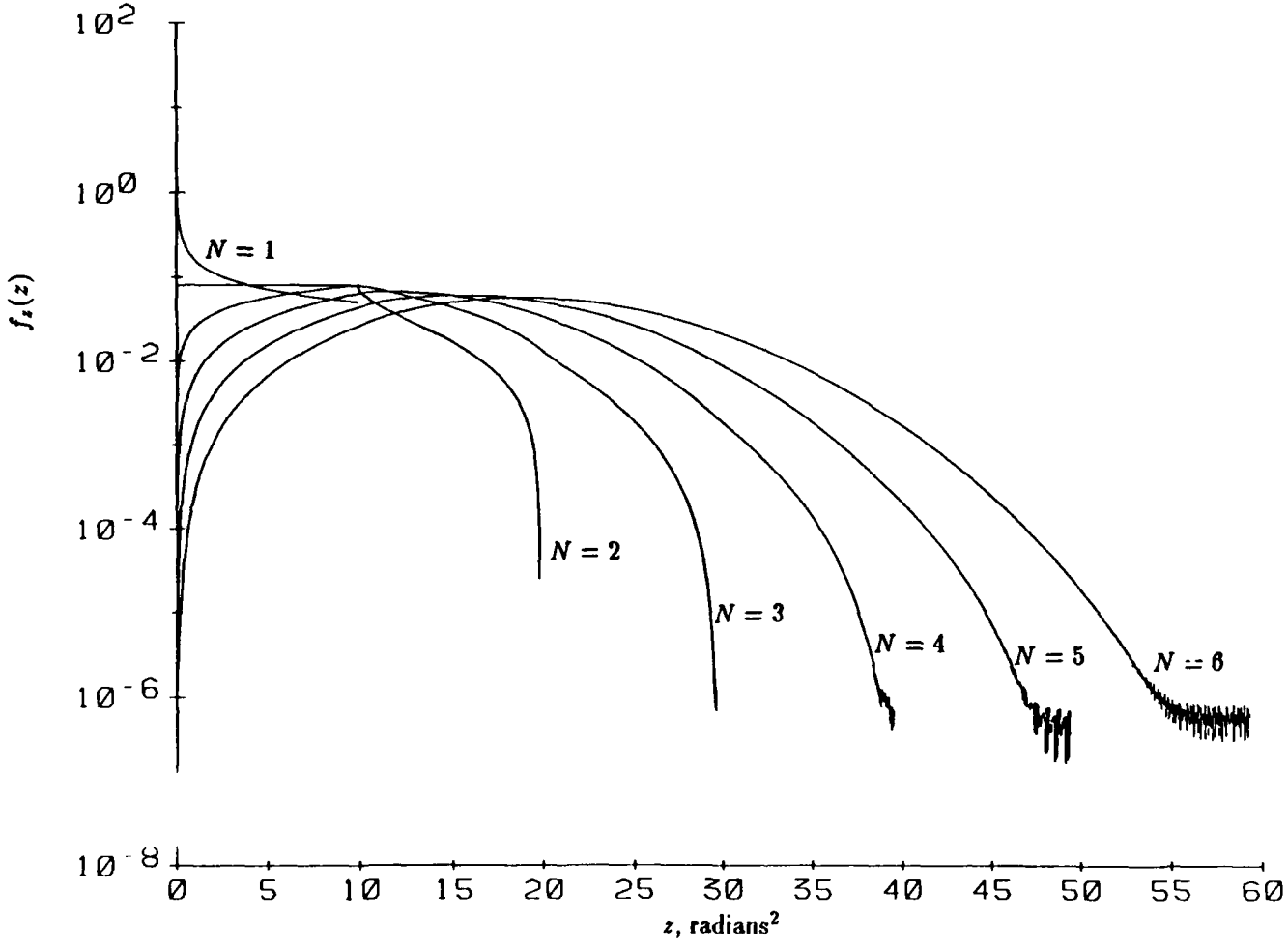

Figure 3.6

$f_z(z)$, Summation (Convolution) pdf's,
for 1 through 6 samples, $k_0 = 0.0$ and $\phi_0 = 0.0$

the regression approximations of the last section. Due to their extremely low magnitude, they do not contribute any significant error.

3.2.1.7 Fourth Transformation, $f_{S^2_\phi}(S^2_\phi)$

It was shown in section 3.2.1.1,[15,24] that the division transformation increases the magnitude and decreases the width N-fold. This is shown in figure 3.7 for the pdf's of figure 3.6. Note that the number of samples starts at 2, corresponding to the minimum number of samples allowable $N-1$. Unlike the convolution operation to find the sample mean in section 3.2.1.2, the abscissa boundaries of the sample variance pdf's are not identical. As the number of samples increases, the widths decrease and converge to π^2. This results from unbiased estimates of the actual variance as per the sample variance normalization discussion in section 3.1.

3.2.2 Theoretical Model Results

In section 3.2.1, the convolution/transformation technique was reviewed in detail for $k_0 = 0$ and $\phi_0 = 0$. Sample variance pdf's for different values of k_0 will now be illustrated using the same method. Intermittent steps will not be shown. Sample variance pdf plots with $\phi_0 = 0$ and 2 through 10 samples, for $k_0 = 0.5$ and $k_0 = 0.9$, are shown in figures 3.8 and 3.9, respectively.

3.3 Monte Carlo Method

In order to verify the results of section 3.2, Monte Carlo estimates of the angle sample variance pdf are computed. In this section the Monte Carlo method will be described. Monte Carlo results will be shown through comparisons with the theoretical model in section 3.4.

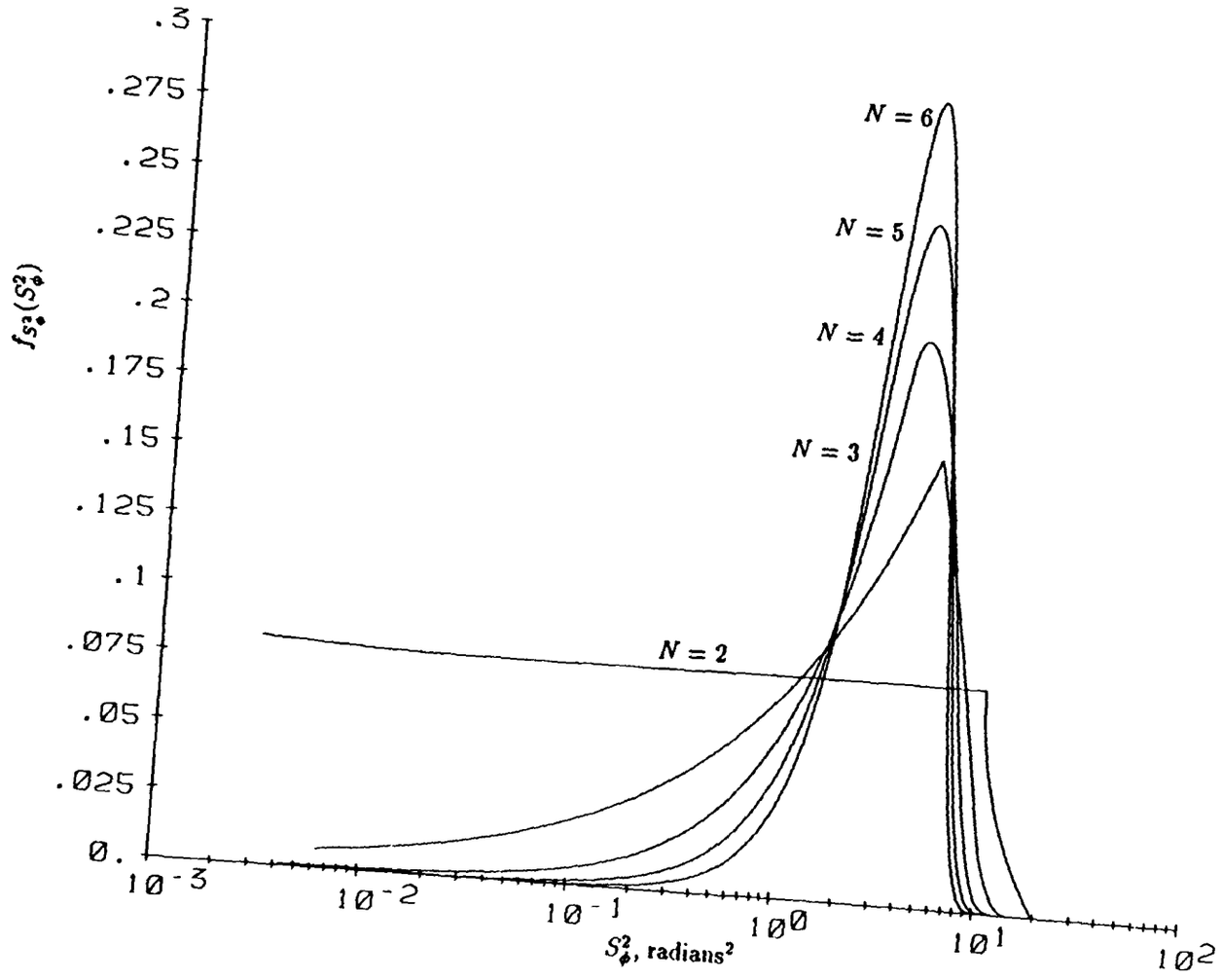

Figure 3.7

$f_{S^2_\phi}(S^2_\phi)$, Electrical Phase Difference Sample Variance pdf's, for 2 through 6 samples, $k_0 = 0.0$ and $\phi_0 = 0.0$

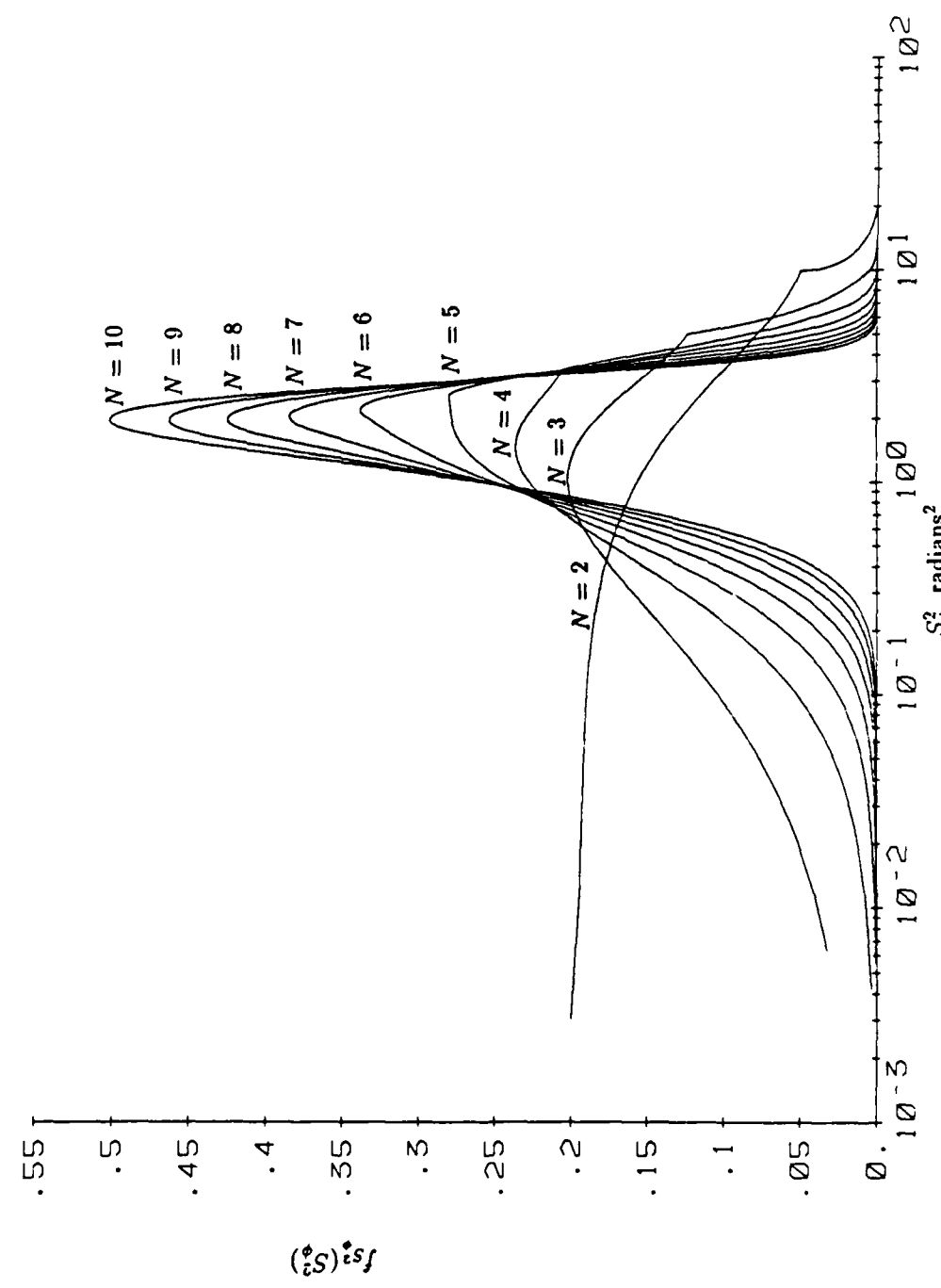

Figure 3.8

$f_{S^2_\phi}(S^2_\phi)$, Electrical Phase Difference Sample Variance pdf's, for 2 through 10 samples, $k_0 = 0.5$ and $\phi_0 = 0.0$

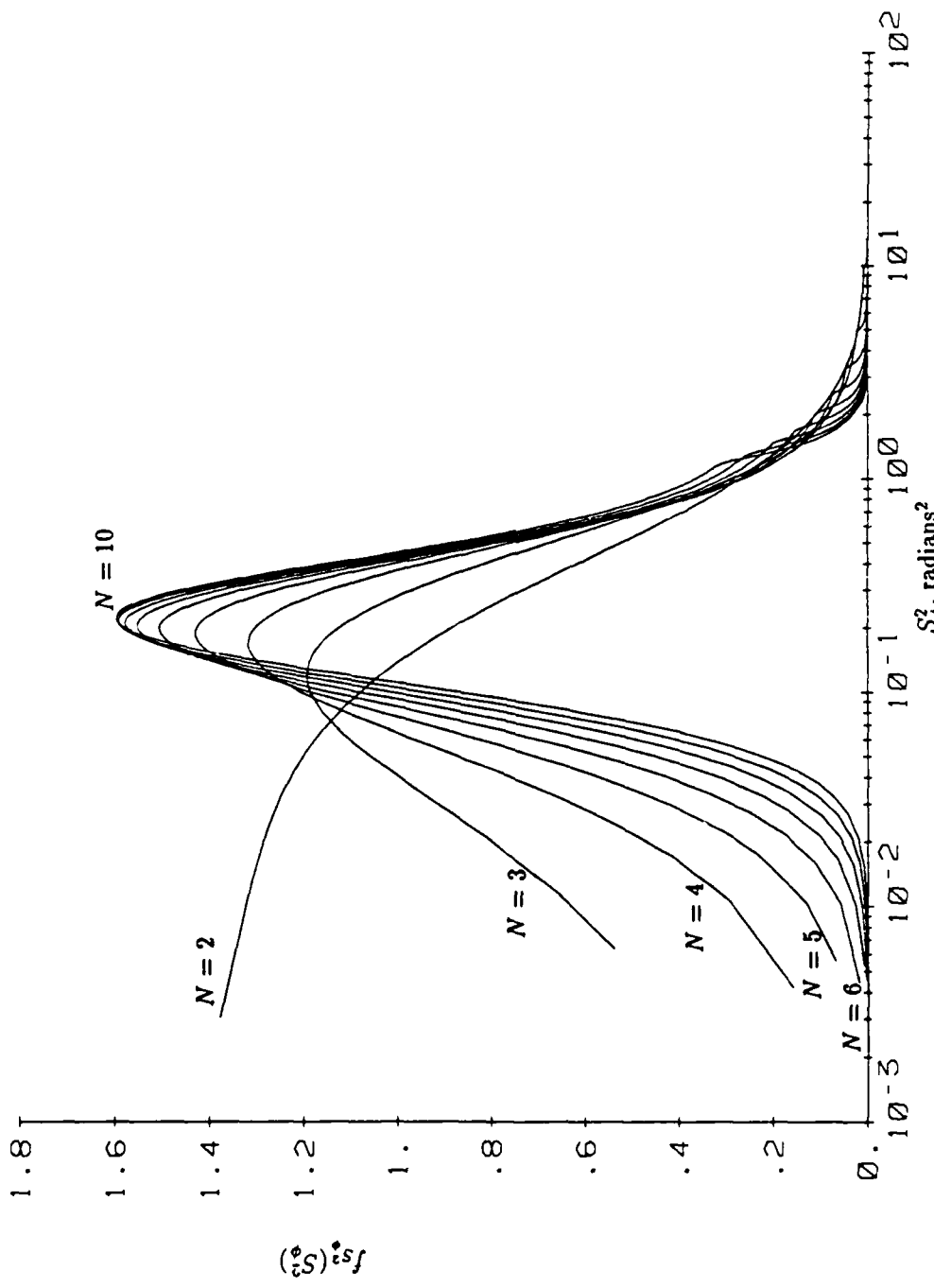

Figure 3.9

$f_{S^2_\phi}(S^2_\phi)$, Electrical Phase Difference Sample Variance pdf's, for 2 through 10 samples, $k_0 = 0.9$ and $\phi_0 = 0.0$

3.3.1 Methodology

By generating a large numbers of random samples which are realizations of the electrical phase difference (angle) pdf of Rainal[17] and substituting these values into equation 3.1, epd samples with correct variance can be synthesized. In order to match the statistically independent assumption of the theoretical pdf's in section 3.2, the mean will be found from a separate set of samples. Effects of correlation between the sample mean and variance will be explored in chapter 4.

3.3.1.1 Random Number Generation

Two methods were explored to generate statistically independent samples which obey the epd pdf. These were inversion[4] and eigenvalue deconvolution.[19]

The inversion method was difficult to work with given the epd pdf because the distribution function equation could not be inverted in closed form. Interpolation between known points did not give satisfactory results.

Statistically independent samples which obey the epd pdf were generated using eigenvalue deconvolution. The basis for the deconvolution is Rainal's derivation of the epd pdf. In doing so, Rainal develops a 4 X 4 covariance matrix M between two vectors N_a and N_b ($N_a = N_1 + jN_2$ and $N_b = N_3 + jN_4$), based upon the most probable electrical phase difference ϕ_0 and the SIR term k_0.[17] The random phase difference is described by the phase angle between these two vectors, i.e.

$$\phi = \tan^{-1} \frac{Im(N_a N_b^*)}{Re(N_a N_b^*)}. \tag{3.25}$$

The four coordinates (eigenvectors) of the two vectors N_a and N_b are zero-mean Gaussian processes with variances equal to each of the four eigenvalues. By

iteratively generating N sets of random realizations of these processes, N random numbers can be generated.[19] A pdf of random variables about the actual pdf for $k_0 = 0.6$ is shown in figure 3.10. The dashed line is a normalized histogram of the random numbers.

3.4 Theoretical/Monte Carlo Results Comparison

Comparative plots of the theoretical versus Monte Carlo results for 4 and 10 samples for $k_0 = 0.0, 0.5$ and 0.9 are shown in figures 3.11, 3.12 and 3.13, respectively. What appears to be a higher degree of error when for $k_0 = 0.9$ in figure 3.13 is caused by the histogram resolution of the Monte Carlo estimates. The samples were put into 250 evenly spaced slices, such that the narrower the width of the theoretical pdf, the lower the comparative resolution of the Monte Carlo pdf.

3.5 Analysis

As can be expected, the mean of the sample variance decreases as k_0 increases, thus signifying existence of a compact scatterer. Theoretical angle sample variance pdf expected values versus actual angle variance, from figure 2.6, are shown in figure 3.14. As the number of samples increases, the expected value of the sample variance converges towards the actual variance shown in figure 2.6. Angle sample variance plots for $k_0 = 0.0$ through 0.9 for $4, 6$ and 8 samples are shown in figures 3.15 through 3.17, respectively.

Due to the significant shift of the sample variance peak (figures 3.15 through 3.17) and mean towards the ordinate axis (figure 3.14), these pdf's can be effectively used as a means to characterize angular spread.

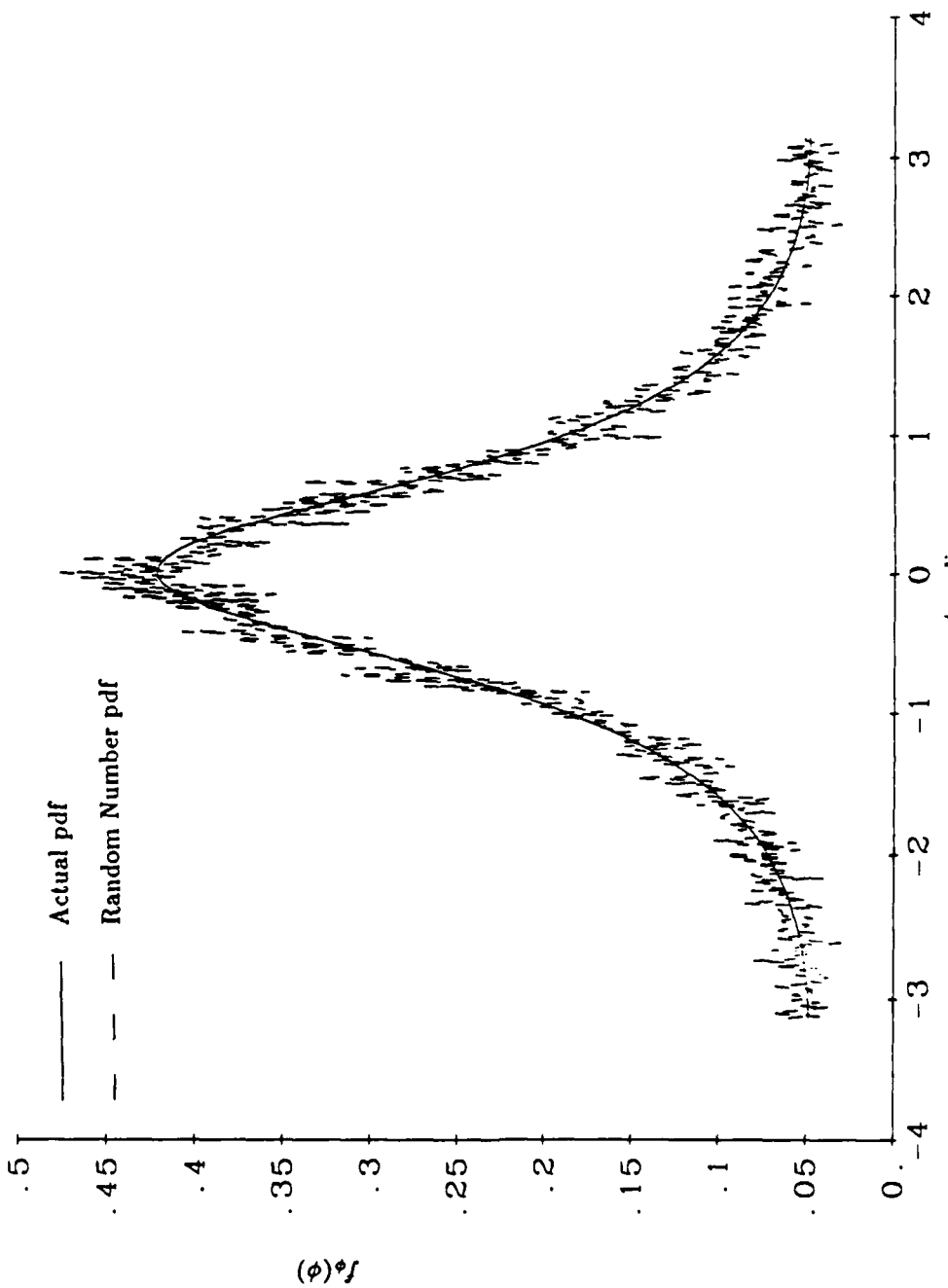

Figure 3.10

$f_\phi(\phi)$, Comparison of Monte Carlo Estimate epd pdf to Actual epd pdf, for $k_0 = 0.6$ and $\phi_0 = 0.0$

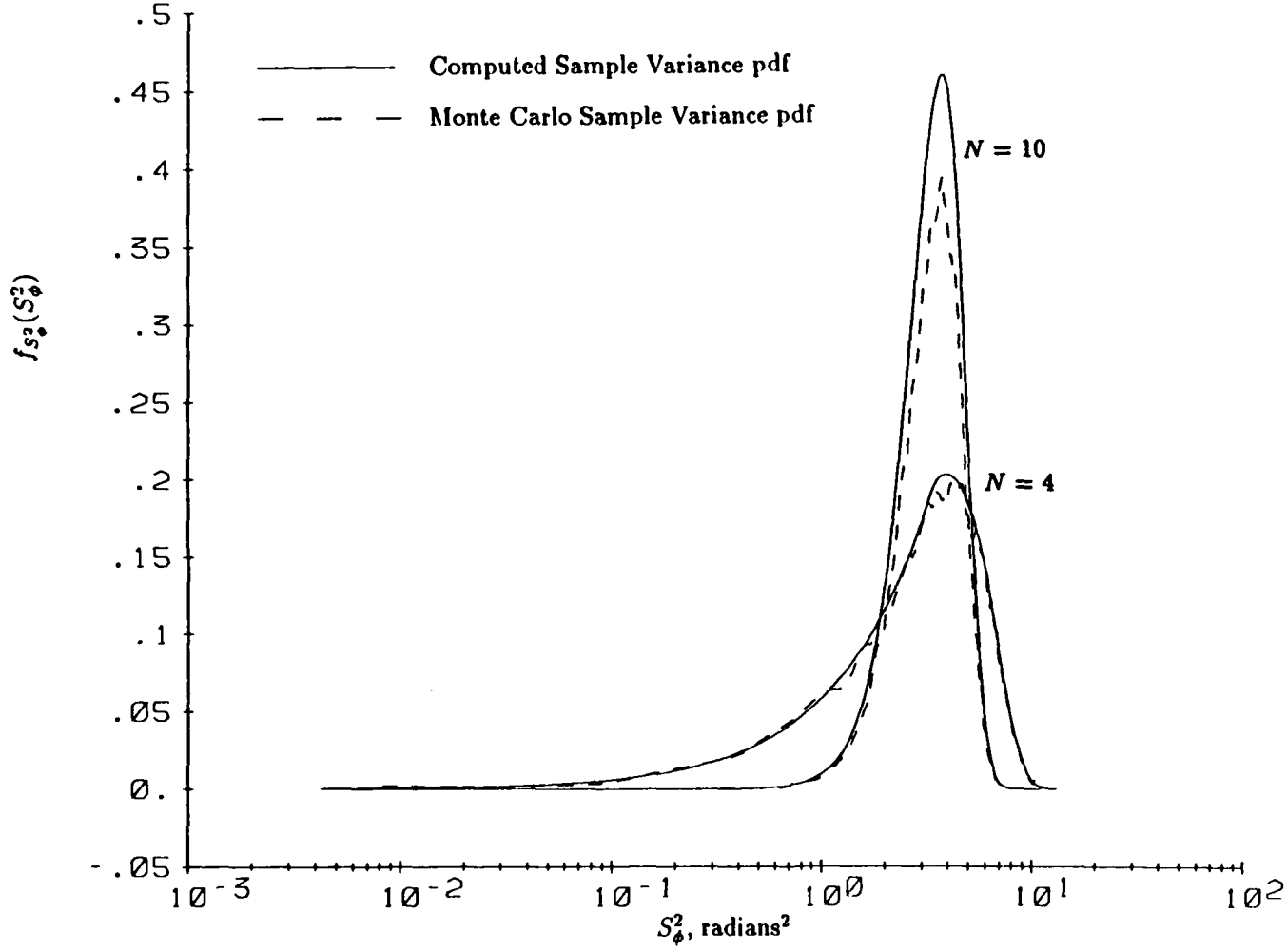

Figure 3.11

$f_{S_\phi^2}(S_\phi^2)$, Comparison of Monte Carlo Sample Variance pdf's to Computed Sample Variance pdf's, for 4 and 10 samples, $k_0 = 0.0$ and $\phi_0 = 0.0$

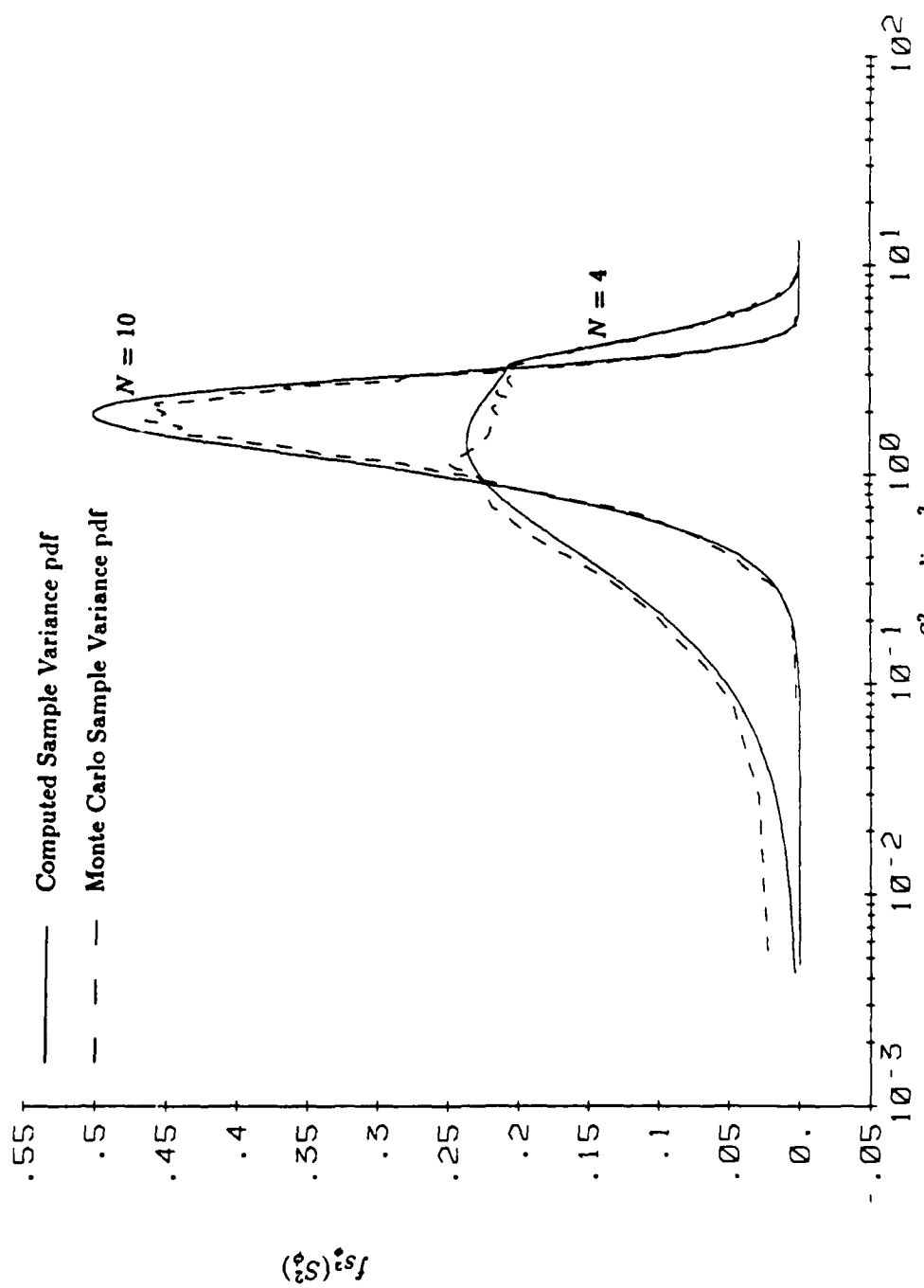

Figure 3.12

$f_{S^2_\phi}(S^2_\phi)$, Comparison of Monte Carlo Sample Variance pdf's to Computed Sample Variance pdf's, for 4 and 10 samples, $k_0 = 0.5$ and $\phi_0 = 0.0$

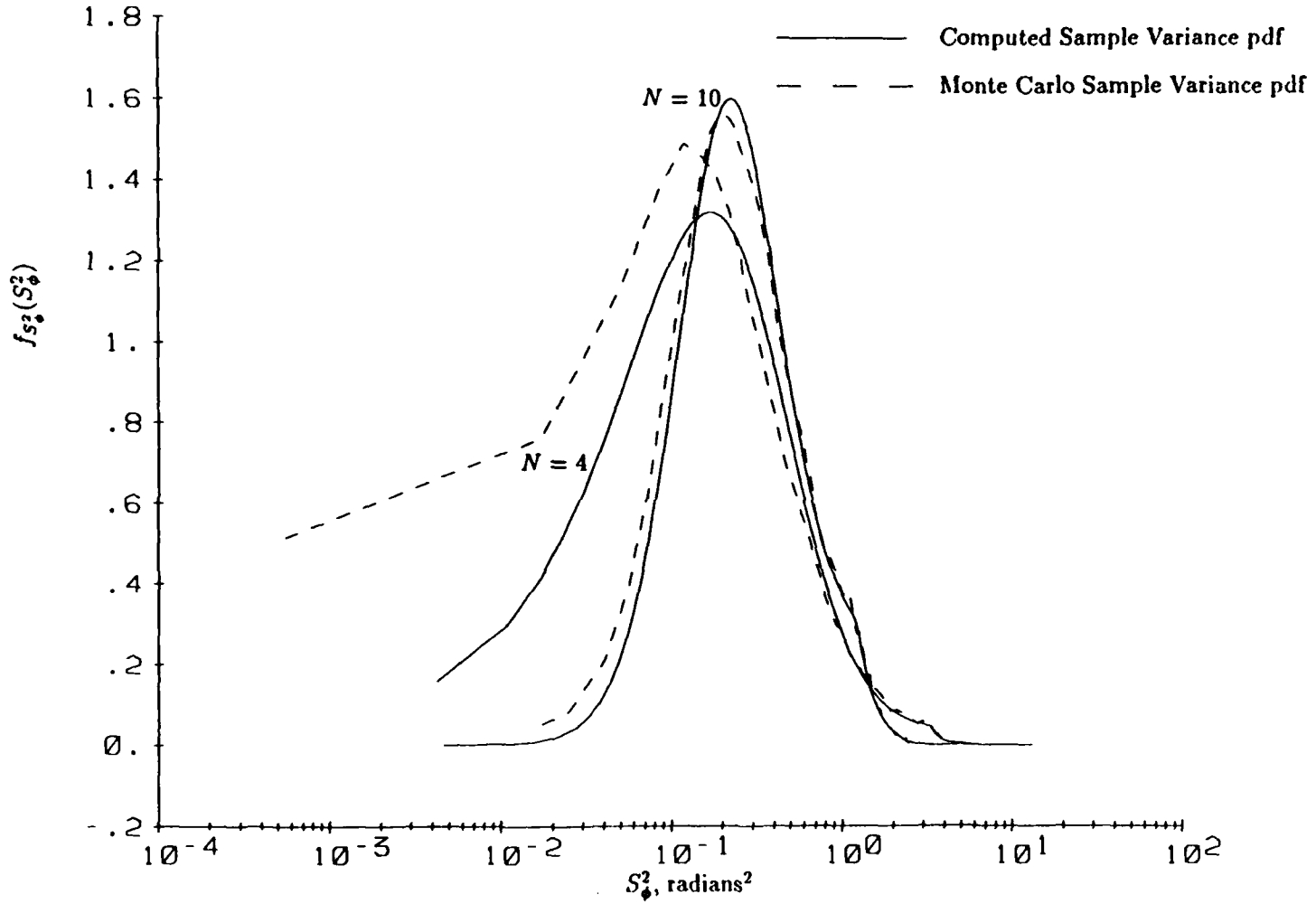

Figure 3.13

$f_{S_\phi^2}(S_\phi^2)$, Comparison of Monte Carlo Sample Variance pdf's to Computed Sample Variance pdf's, for 4 and 10 samples, $k_0 = 0.9$ and $\phi_0 = 0.0$

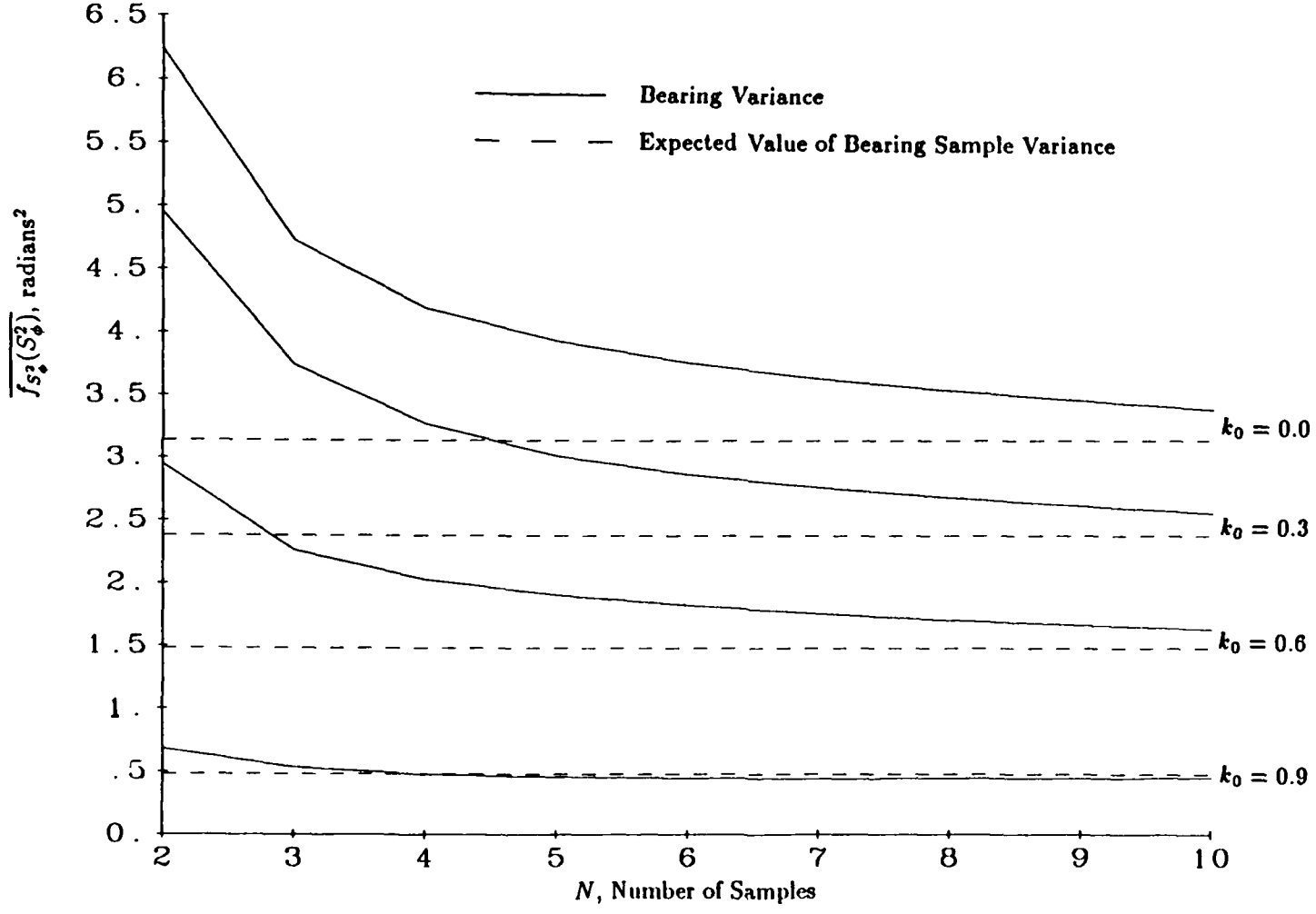

Figure 3.14

Bearing Sample Variance Mean Values,
for $k_0 = 0.0$ through 0.9 in 0.3 increments and 2 through 10 samples

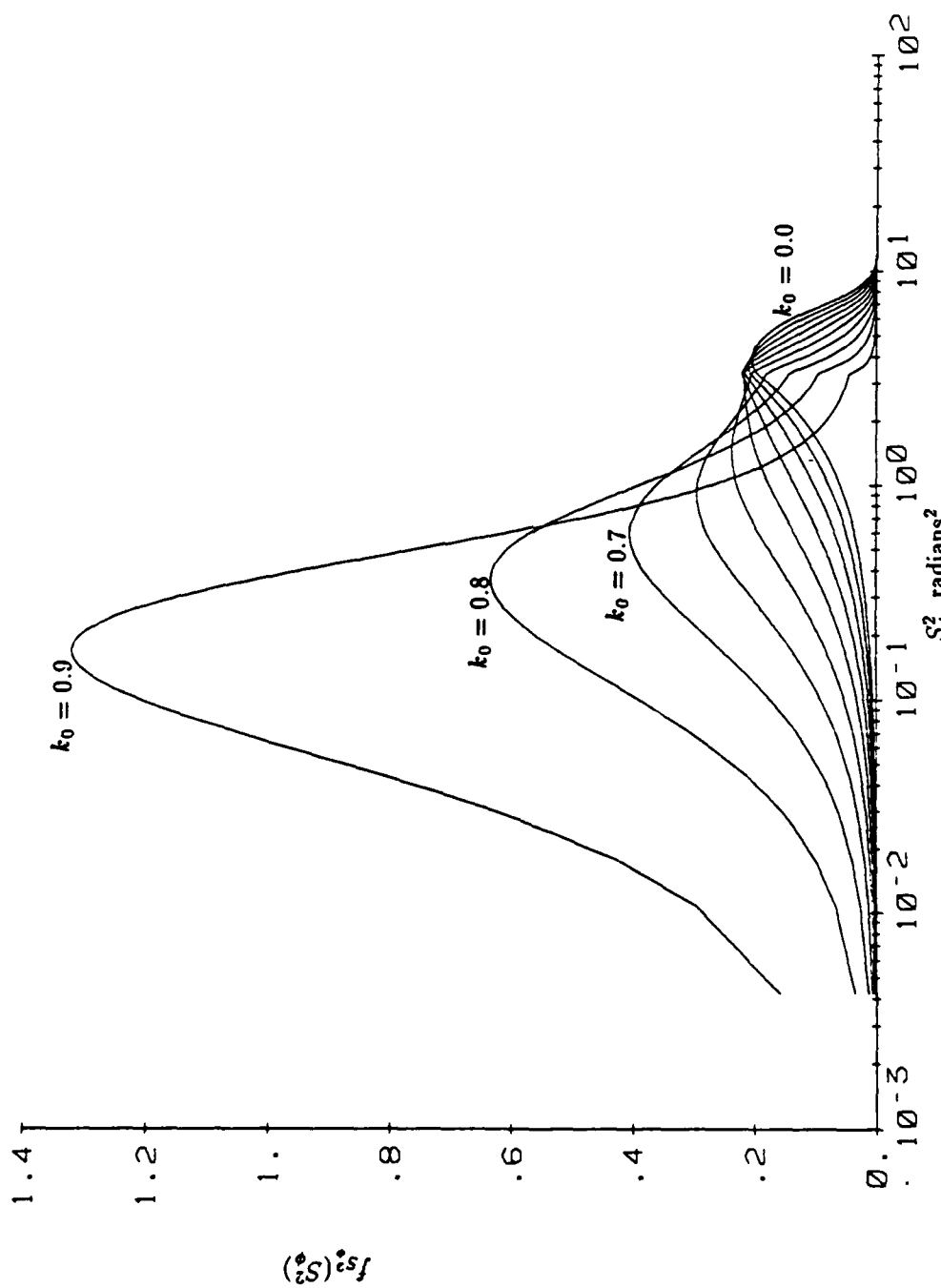

Figure 3.15

$f_{S^2_\phi}(S^2_\phi)$, Electrical Phase Difference Sample Variance pdf's, for 4 samples, $k_0 = 0.0$ through 0.9, and $\phi_0 = 0.0$

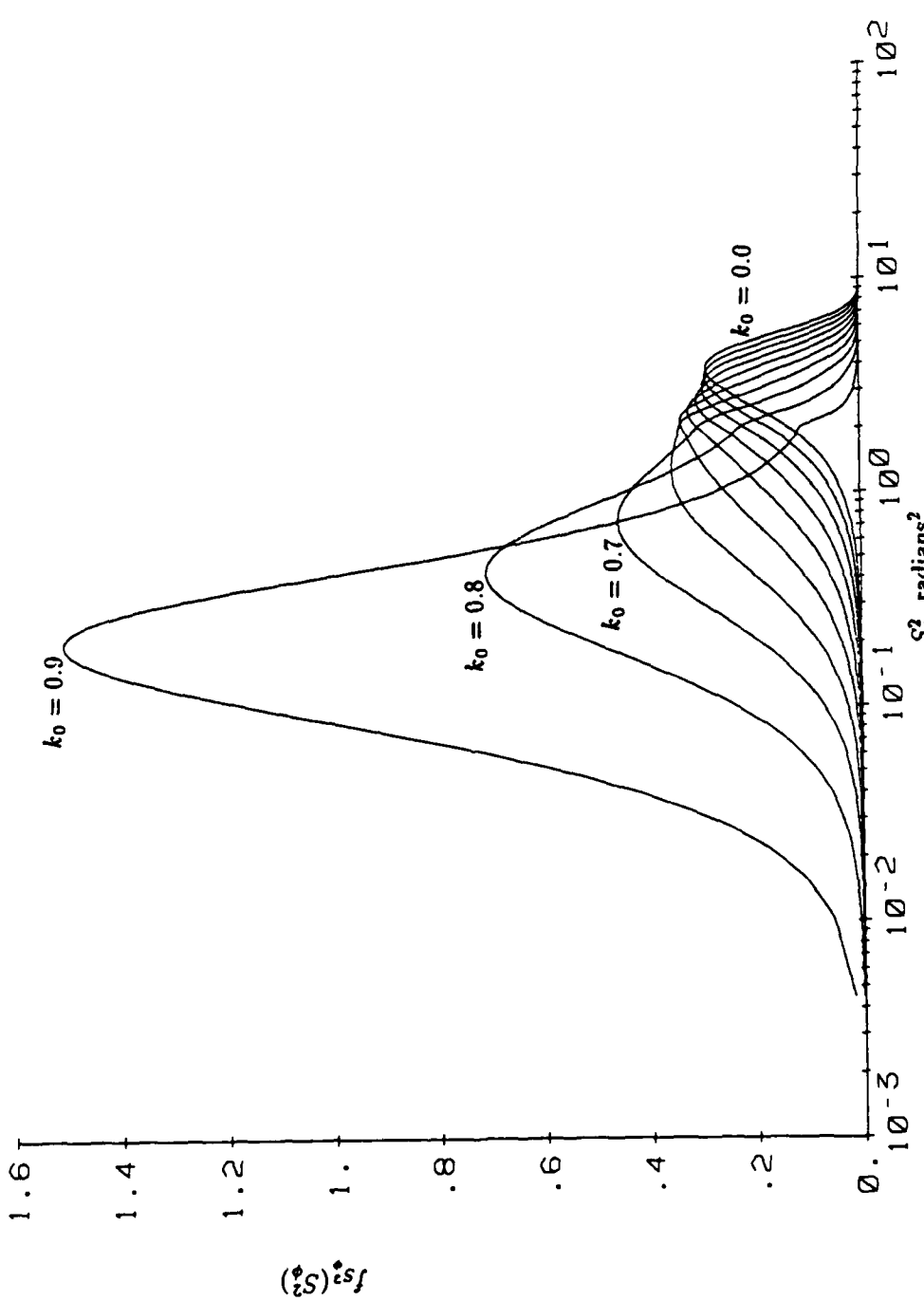

Figure 3.16

$f_{S^2_\phi}(S^2_\phi)$, Electrical Phase Difference Sample Variance pdf's, for 6 samples, $k_0 = 0.0$ through 0.9, and $\phi_0 = 0.0$

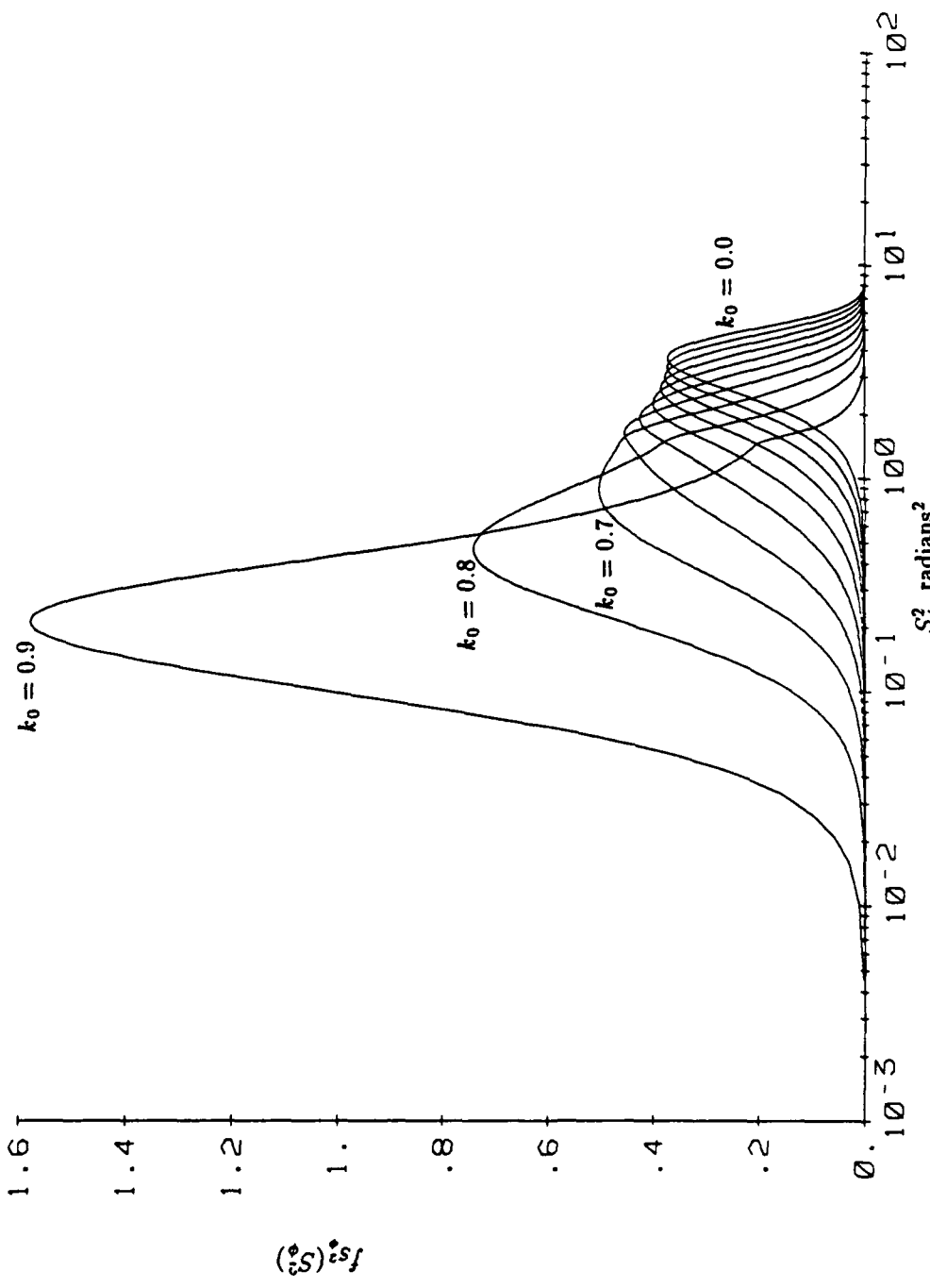

Figure 3.17

$f_{S^2_\phi}(S^2_\phi)$, Electrical Phase Difference Sample Variance pdf's, for 8 samples, $k_0 = 0.0$ through 0.9, and $\phi_0 = 0.0$

As the number of samples N increases, the "sample variance" pdf approaches the variance pdf given by equation 2.31 and shown in figure 3.14.

The Monte Carlo method does not have any bias since the sample variance was carried out directly on an unbiased sample set. However, the transformation/convolution method does exhibit some bias. Errors were evaluated by taking the area of the pdf's in each step. The dominant error comes from the squaring operation of section 3.2.1.5 and the discretization operation of section 3.2.1.5.1.

In the squaring operation, the first abscissa value, w, must approach 0 but can not be equal to 0. This is due to the transformation operation of equation 3.24, wherein the square root of the abscissa value is the divisor, thus making the ordinate value $f_y(y) = \infty$ at $w = 0$, or equivalently the probability that $w = 0$ is zero, $f_w(0) = 0$. The first abscissa value must be adjusted dependent upon the SIR, which is proportional to the slope, and the number of data points. The first abscissa value was set at $w = 0.003$, which gave sample variance areas of 1 ± 10^{-3} for $k_0 = 0.5$ with $N = 1$ through 10. Optimally, the first abscissa value should be adjusted for each value of k_0.

The discretization method uses regression techniques to interpolate points. Thus the quality of the interpolation is a function of the estimated regression coefficients. In this case, the slope and curvature of the known set of data played the dominant role in the quality of the fit (low quality with high slope and curvature). The number of points per regression and order of the regression were tuned by process of elimination such that there was minimal variation about the actual values.

As a result of these calibrations, the worst case sample variance area

(which should optimally be 1.) was at 10 samples with $k_0 = 0.9$, and was equal to 0.9857 (1.43% error).

Chapter 4

CORRELATION EFFECTS

4.1 Introduction

Given a finite data set, it is necessary to find the sample variance from the same set of data from which the sample mean is found, thus reducing the degrees of freedom by "1."

In finding the sample variance pdf in chapter 3, the sample mean was found from N statistically independent samples, as per equation 3.3. As a result of this operation, the following step, wherein the difference about the sample mean is found in equation 3.4, violates a common sampling scenario in that the sample mean and variance must be statistically independent. The convolution integral is only valid if the pdf's are statistically independent. In other words, if the mean is computed with the same set of data as that which is found about the mean, the assumption that ϕ_i and $\overline{\phi}$ are independent does not hold. This effect is multiplied in equation 3.7, where the difference squared is convolved $N-1$ times. In order to produce useful statistics of sample variance in this situation, correlation between the sample mean and variance must be either compensated for or modeled.

There is no attempt in this thesis to model these effects theoretically due to their computational complexity. However, such effects can be modeled with ease using the Monte Carlo method of section 3.3. The effects will be comparatively illustrated between the uncorrelated theoretical pdf's and correlated Monte Carlo empirical distribution functions (edf's) in section 4.2. Recommendations

for reducing correlation effects will be given in section 4.3.

4.2 Monte Carlo Correlation Model

Comparative plots of the uncorrelated theoretical model of section 3.2 and the Monte Carlo correlation models for 4, 6 and 10 samples, with $k_0 = 0.0, 0.5$ and 0.9 are shown in figures 4.1, 4.2 and 4.3, respectively. These values provide a good model because (1) the assigned values for k_0 represent extremes and (2) the assigned numbers of samples will provide a reasonable range and yet not experience too much overlap with multiple plots on the same graph.

At low sample size, the uncorrelated model exhibits a lower variance, however, as the number of samples increases, the two curves converge. This behavior is to be expected since the correlated samples are closer to the mean value and thus exhibit a lower variance.

4.3 Correlation Compensation Recommendations

There are potential compensations which can be made for correlation effects. Such compensations can either make the sample mean and sample variance about the sample mean uncorrelated or approach being uncorrelated.

Often, there may be several sets of wide sense stationary data which arrive chronologically. In such cases, the sample mean can be found from the first set of data and the sample variance about the mean can be found using the samples of the second set of data about the sample mean of the first set of data. Repeating this procedure with each additional set of data would provide statistical independence between the sample mean and sample variance about the sample mean.

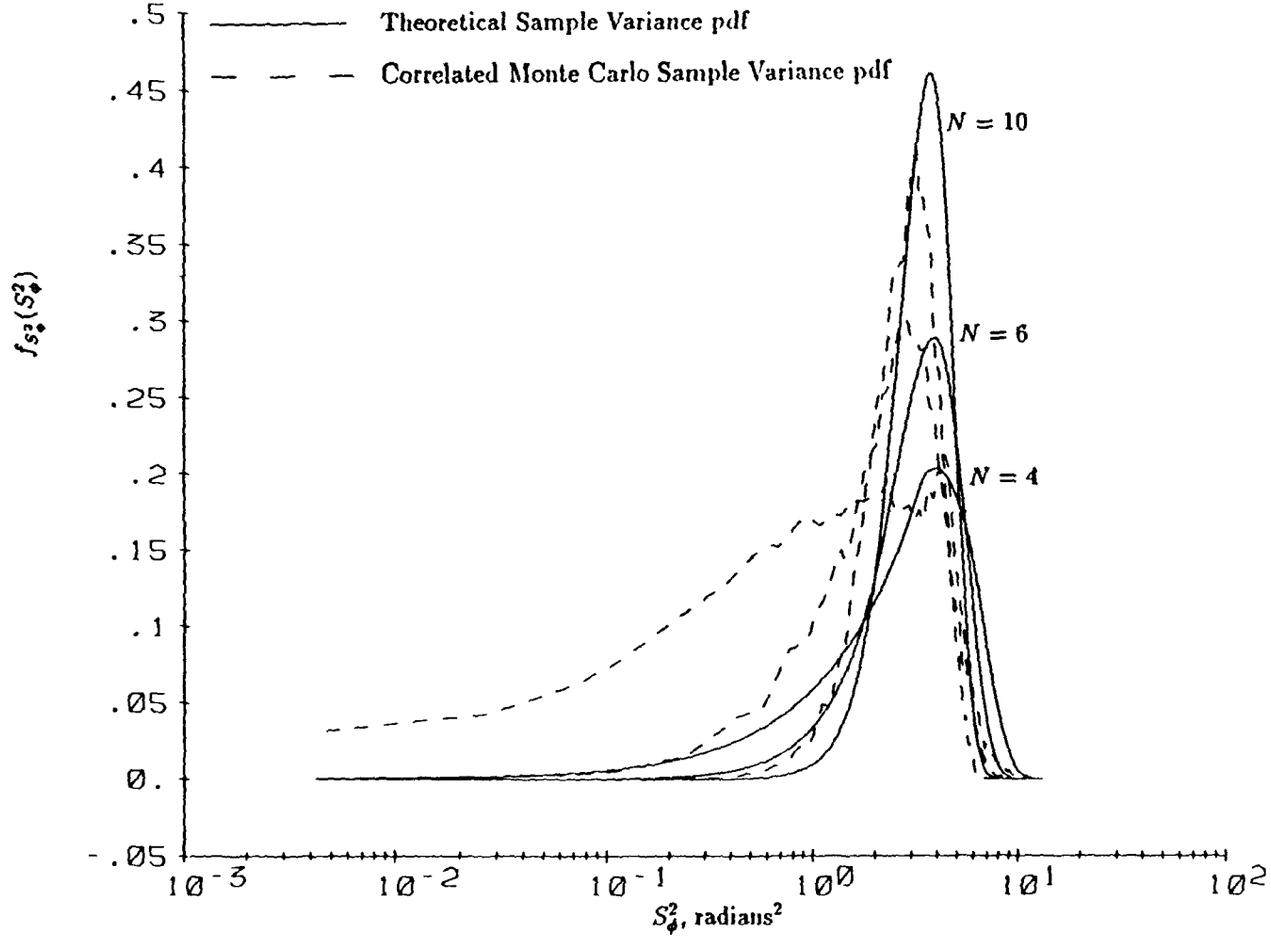

Figure 4.1

$f_{S_\phi^2}(S_\phi^2)$, Comparison of Theoretical Model to Correlated Monte Carlo Model, for 4, 6 and 10 samples, $k_0 = 0.0$, and $\phi_0 = 0.0$

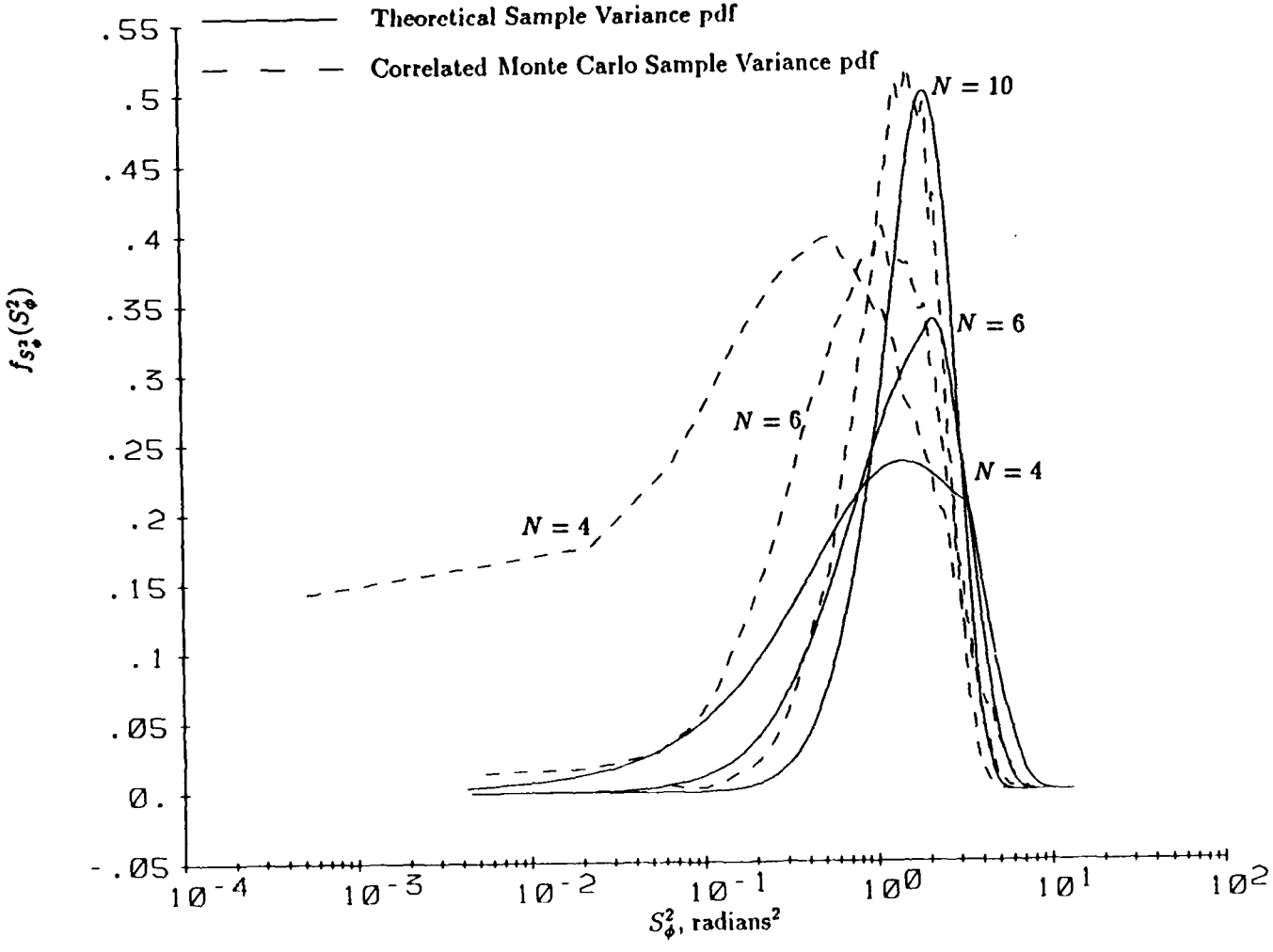

Figure 4.2

$f_{S^2_\phi}(S^2_\phi)$, Comparison of Theoretical Model to Correlated Monte Carlo Model, for 4, 6 and 10 samples, $k_0 = 0.5$, and $\phi_0 = 0.0$

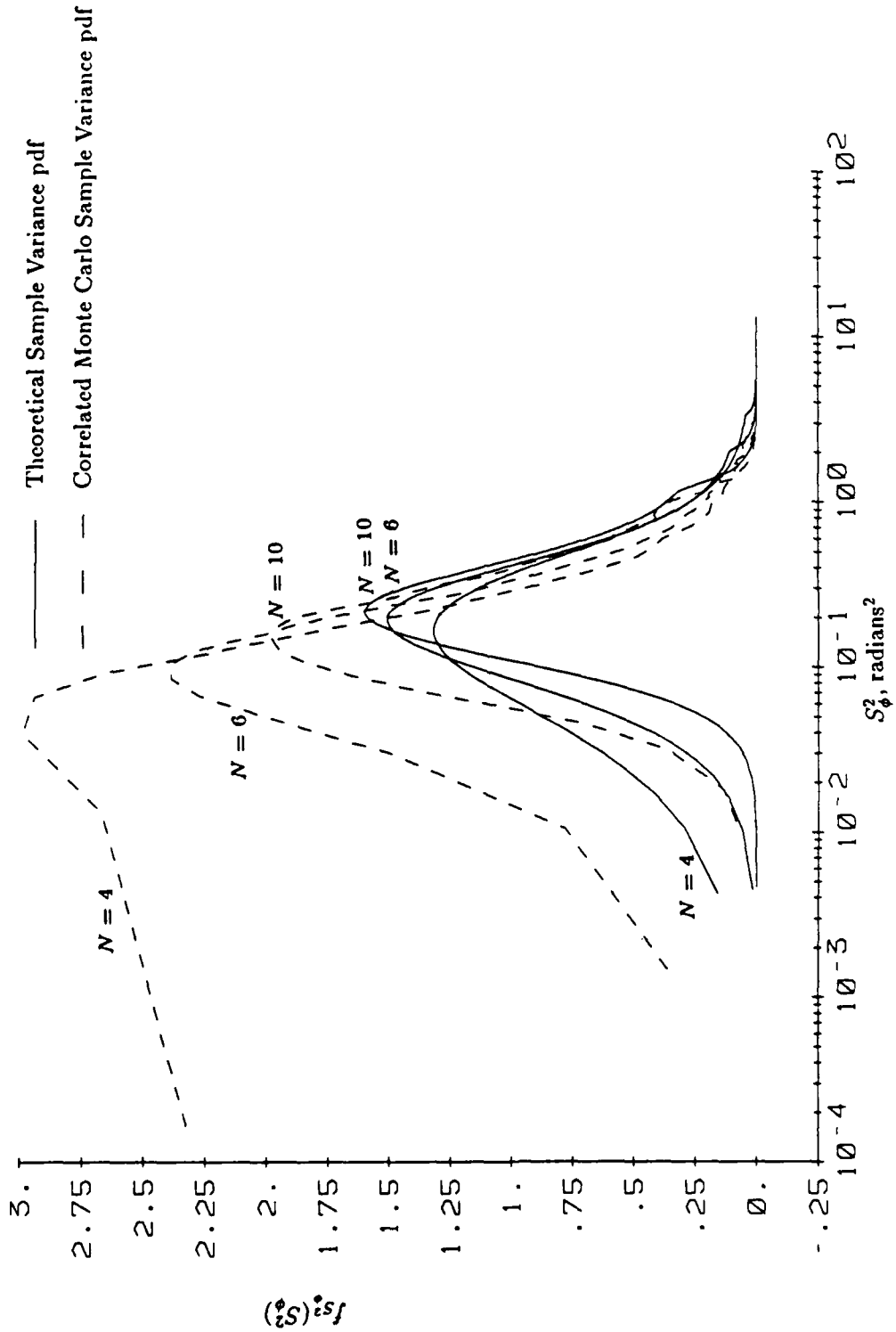

Figure 4.3

$f_{S^2_\phi}(S^2_\phi)$, Comparison of Theoretical Model to Correlated Monte Carlo Model, for 4, 6 and 10 samples, $k_0 = 0.9$, and $\phi_0 = 0.0$

Given one sample set, one can find the sample mean with part of the sample set, and then find the difference about the sample mean with the remainder of the sample set. Obviously though, this reduces the effective sample set.

When there are correlation effects, the Monte Carlo correlation model provides useful results for small data sets ($\approx N < 8$) because of dominant errors in the statistically independent theoretical model. However, estimation techniques should be evaluated for each specific case, and if usable, the theoretical model (transformation/convolution) would be the most simplistic approach in attaining the best results due to its smooth curvature. For example, if there is a large number of samples, the theoretical model would provide a close approximation.

Chapter 5

SUMMARY AND CONCLUSIONS

5.1 Summary

It has been shown that the angle sample variance of a two-element array can effectively be utilized as a means of characterizing the azimuthal support of spatially spread scattering processes.

In chapter 2, the scattering mechanisms of spatially coherent and diffuse processes incident upon a two-element array have been modeled. In section 2.3, an expression describing the epd pdf in terms of the component scattering functions was developed. An idealized example illustrated that the most probable electrical phase difference is biased by the diffuse scattering process distribution and not the white Gaussian noise.[19] Through an examination of the electrical phase difference pdf of Middleton[13] and Rainal,[17] it has been shown that the angle sample variance is inversely proportional to k_0. Under low levels of diffuse scattering and noise, spatially coherent processes will exhibit a low angle sample variance.

The significant contribution of this thesis is the presentation of a multi-step transformation process to find the sample variance pdf given the pdf of a single realization, which is the angle pdf for the case illustrated. The angle sample variance pdf's were shown to be inversely proportional to k_0 in chapter 3.

A primary assumption in the development of the angle sample variance pdf's was that the sample mean and sample variance are uncorrelated, i.e. N degrees of freedom. Correlation effects upon the angle sample variance pdf were

shown through Monte Carlo techniques in chapter 4. At low numbers of samples there was decreased variance, and as the number of samples increased (≈ 8) there was divergence towards the uncorrelated model.

5.2 Recommendations

Recommendations for future work include the following:

1. Development of closed form solutions for the correlated theoretical model and the uncorrelated Monte Carlo model, which would require development of a correlation matrix. It is noteworthy that the sample variance pdf's resemble both chi-square and Rician density functions and could potentially be described in terms of such.

2. Extension to Doppler spread processes.

3. Introduce temporal and spatial correlation.

4. Extension to wideband processes.

REFERENCES

[1] Altes, T. L., Titlebaum, E. L., "Graphical Derivations of Radar, Sonar, and Communication Signals," *IEEE Transactions Aerospace and Electronic Systems*, Vol. AES-11, No. 1, pp. 38-44, January 1975.

[2] Bendat, J. S., Piersol, A. G., *Random Data - Analysis and Measurement Procedures*, pp. 75 and 102-6, New York, NY: John Wiley and Sons, Inc., 1986.

[3] Burdic, W. S., *Underwater Acoustic System Analysis*, pp. 126-54 and 361-73, Englewood Cliffs, NJ: Prentice-Hall, Inc., 1984.

[4] Canavos, G. C., *Applied Probability and Statistical Methods*, p. 289, Boston, MA: Little, Brown and Company Limited, 1984.

[5] Costas, J. P., "A Study of a Class of Detection Waveforms Having Nearly Ideal Range-Doppler Ambiguity Properties," *Proceedings of IEEE*, Vol. 72, No. 8, pp. 996-1009, August 1984.

[6] DeFatta, D. J., Lucas, J. G., Hodgkiss, W. S., *Digital Signal Processing - A System Design Approach*, pp. 53-5, New York, NY: John Wiley and Sons, Inc., 1988.

[7] Glisson, T. H., Black, C. I., Sage, A. P., "On Sonar Signal Analysis," *IEEE Transactions Aerospace and Electronic Systems*, Vol. AES-6, No. 1, pp. 37-49, January 1970.

[8] Golomb, S. W., Taylor, H., "Constructions and Properties of Costas Arrays," *Proceedings of IEEE*, Vol. 72, No. 9, pp. 1143-1163, August 1984.

[9] Green, P. E., Jr., "Radar Measurements of Target Scattering Properties," In J. V. Evans and T. Hagfors (Eds.), *Radar Astronomy*, New York, NY: McGraw-Hill, Inc, 1968.

[10] Laval, R., Labasque, Y., "Medium Inhomogeneities and Instabilities: Effects on Spatial and Temporal Processing," *Underwater Acoustics and Signal Processing*, pp. 41-70, D. Reidel Publishing Company, Dordrecht, Holland, 1981.

[11] Marple, S. L., Jr., *Digital Spectral Analysis with Applications*, pp. 37-42, Englewood Cliffs, NJ: Prentice-Hall Inc., 1987.

[12] Merchant, C. C., *Detection of a Dual Channel Differential Phase Modulated Signal in Correlated Noise*, MS Thesis, The Pennsylvania State University, pp. 26-31, August 1982.

[13] Middleton, D., *Introduction to Statistical Communications*, pp. 397-409, McGraw-Hill, New York, NY, 1961.

[14] Middleton, D., "A Statistical Theory of Reverberation and Similar First-Order Scattered Fields," *IEEE Transactions on Information Theory, Part I*, Vol. IT-13, No. 3, pp. 384-8, July, 1967.

[15] Papoulis, A., *Probability, Random Variables, and Stochastic Processes*, 2nd ed., pp. 95-104, New York, NY: McGraw-Hill, Inc., 1984.

[16] Peebles, P. Z., *Probability, Random Variables, and Random Signal Principles*, 2nd ed., pp. 102-3, New York, NY: McGraw-Hill, Inc., 1987.

[17] Rainal, A. J., "Monopulse Radars Excited by Gaussian Signals," *IEEE Transactions on Aerospace and Electronic Systems*, Vol. AES-2, No. 3, pp. 337-345, May 1966.

[18] Ricker, D. W., "Small Aperture Angle Measurement for Active Echo Location Systems," *IEEE Transactions Aerospace and Electronic Systems*, Vol. AES-22, No. 4, pp. 380-388, July 1986.

[19] Ricker, D. W., The Pennsylvania State University, Applied Research Laboratory, Personal communication.

[20] Rihaczek, A. W., *Principles of High-Resolution Radar*, New York, NY: McGraw-Hill, Inc., 1969.

[21] Titlebaum, E. L., "Echolocation Systems in Nature; A Theory of Optimum Insensitivity to Motion for Bats," *Ultrasonic Symposium Proceedings*, IEEE Catalog Number 78CH 1344 - 1SU, 1978.

[22] Urick, R. J., *Principles of Underwater Sound*, 3rd ed., pp. 202-33, New York, NY: McGraw-Hill, Inc., 1983.

[23] Van Trees, H. L., *Detection, Estimation, and Modulation Theory, Part III*, New York, NY: John Wiley and Sons, Inc., 1971.

[24] Whalen, A. D., *Detection of Signals in Noise*, pp. 13-14 and 126-40, New York, NY: Academic Press, Inc., 1971.

[25] Woodward, P. M., *Probability and Information Theory with Applications to Radar*, Oxford, England: Pergamon, 1964.

[26] Ziomek, L. J., *Underwater Acoustics - A Linear Systems Theory Approach*, pp. 7-28, New York, NY: Academic Press, Inc., 1985.

[27] Ziomek, L. J., *A Scattering Function Approach to Underwater Acoustic Detection and Signal Design*, Ph.D. Dissertation, The Pennsylvania State University, pp. 50-66, 1981.